Curved quasi-steady detonations:

Asymptotic analysis and detailed chemical kinetics

R. Klein

Institut für Technische Mechanik, RWTH Aachen

Templergraben 64, 52056 Aachen, Germany

J. C. Krok, J. E. Shepherd

GALCIT, California Institute of Technology, Pasadena CA 91125, USA

May 17 1995

GALCIT REPORT FM 95-04

ABSTRACT

We consider the problem of slightly-curved, quasi-steady diverging detonation waves. For sufficiently small curvature, the reaction zone structure equations can be formulated as a two point boundary value problem for solutions containing a sonic point. Analytical solutions to this boundary value problem are obtained for the case of a one-step Arrhenius reaction in the limit of high activation energy. The analytic solution results in a nonlinear relationship between detonation velocity and curvature. For extremely small curvature, this relationship is consistent with previous linear analyses, whereas in the nonlinear regime it predicts a critical maximum curvature, beyond which no quasi-steady solutions with a sonic point can be found. We also analyse the curved detonation structure for the gaseous fuel-oxidizer combination of H_2 and O_2 with various diluents. Using a standard shooting method we generate numerical solutions of the two-point boundary value problem based on realistic thermochemistry and a detailed chemical reaction mechanism. Similar to the large activation energy results, the numerical solutions reveal a nonlinear detonation speed-curvature relation and a critical maximum curvature for the existence of quasi-steady solutions. The relation of this critical curvature to the critical scales of multi-dimensional detonation is discussed.

PACS numbers: 47.40-x, 47.70.Fw

I. INTRODUCTION

Detonation waves are observed to be curved in a variety of situations. Initiation by spherical or cylindrical sources, diffraction around a convex corner and the local fronts of unstable detonations are some of the common examples of this phenomenon (see Fig. 1). Detonation waves propagating axially in cylinders of high explosives are curved due to the lateral expansion of the products. Extensive investigations, starting with Wood and Kirkwood,[1] of this problem indicate that under certain conditions, there exists a relationship between a minimum detonation velocity D_s and the wave curvature κ.

This velocity is physically significant since it is only for this value that the steady reaction zone solution can smoothly pass through a sonic point. This can be considered the generalization of the usual Chapman-Jouguet point for planar detonation waves. The physical significance is apparently that stable, self-sustaining waves appear to asymptotically propagate at a velocity close to D_s in many situations. Heuristically, it is argued that for detonation velocities $D > D_s$, there is no sonic point in the reaction zone and flow disturbances traveling upstream from the region behind the detonation can affect the detonation propagation. In most situations, these disturbances are rarefactions and cause the wave to attenuate so that $D \to D_s$. The rate of attenuation decreases as this occurs (see the discussion of the shock change equation on p. 101 of Fickett and Davis[2]) until ultimately a quasi-steady reaction zone containing a sonic point results. The sonic point then effectively isolates the wave from the following flow and the detonation locally propagates with a normal velocity $D_s(\kappa)$, usually just written $D(\kappa)$.

We emphasize that this argument holds as is only for diverging waves, while it fails for

converging ones. A detailed asymptotic analysis of the curvature-induced wave acceleration of converging detonations, which inhibits the establishment of a quasi-steady detonation structure, has been reported by Klein.[3]

Attractive as this picture appears, there is a key difficulty in applying it to detonations as realized in nature. It is well known that for a wide range of reaction mechanisms and rate laws characteristic of gaseous reaction that planar detonation waves are unstable to transverse disturbances for all velocities sufficiently close to the CJ value. This was observed first in the laboratory by White,[4] extensively studied in subsequent experiments,[5] and demonstrated by linear stability analyses[6,7] and a combination of linear stability analysis and numerical simulation.[8] We expect that small amounts of curvature will not suppress this instability and this will be a key obstacle to applications involving gaseous or unstable solid explosives. It may in fact be possible to develop a "renormalized" $D(\kappa)$ relationship that incorporates the effect of the instability but this is merely speculation at the present time.

If we accept the existence of a $D(\kappa)$ relation, then geometrical considerations of the wave front evolution enable the computation of the front position and shape as a function of time without the need to solve for the rest of the flow field. Bdzil and others[9,10] have carried out extensive studies on this notion, which they term *detonation shock dynamics*. This theory utilizes either a measured[11] or computed $D(\kappa)$ relationship to numerically predict[12,13] the detonation front shape evolution. For some high explosives, this appears to be an exceedingly useful approach that reproduces measured wave shapes of diffracting detonations and provides very useful insight into the diameter effect in rate stick experi-

ments.

A particularly significant feature of the rate stick experiment is that the detonation wave "fails" when the stick diameter is below some critical value. Failure in this instance means that the wave velocity decays and the chemical reactions effectively cease to sustain the wave over a long distance of propagation. This has the wider significance that under many situations diffracting detonation waves and curved waves produced by yielding confinement will fail when the curvature exceeds a critical value. In terms of the $D(\kappa)$ model for propagation, this indicates that there is a limiting value of curvature $\kappa_{\max}$, beyond which a sonic point does not appear in the flow for any detonation velocity. However, the relationship between the critical rate stick diameter and the critical wave curvature is not straightforward. Furthermore, it is observed that in diffraction situations, portions of a wave may exceed the critical curvature for some time but ultimately the wave will continue to propagate as a self-sustaining detonation. The prediction of the success or failure of detonation wave initiation and diffraction in general situations is still a largely unsolved problem that requires experimental resolution at the present time. The connection of the general situation to the special case of quasi-steady, slightly-curved waves is tenuous but the appearance of a critical curvature is an hopeful sign and suggests that further analysis is worthwhile.

To date, the $D(\kappa)$ relationships have been based on relatively simple reaction rate laws or determined experimentally for high explosives. For small values of curvature, Klein and Stewart[14] have shown that the most common sort of reaction rate models appropriate to gas phase combustion will lead to a linear relationship between normal detonation velocity

and the curvature, with logarithmic corrections in the case of first-order reactions. These calculations do not predict a limiting critical curvature although this is anticipated on the basis of the critical effects observed in detonation experiments. In fact, in this previous work, Klein and Stewart do consider the same large activation energy Arrhenius kinetics that we use here in Sec. III, yet they perform a *sequential* asymptotic limit where the activation energy becomes large only *after* the small curvature limit has been obtained. This approach is inherently different from the present distinguished limit between the orders of magnitude of curvature and activation energy. This very distinguished limit has independently been considered by Yao and Stewart[15] and, with the additional assumption of a specific heat ratio close to unity, by He and Clavin.[16]

In the present study we analyse the problem of $D(\kappa)$ relationships for systems described by either one-step Arrhenius kinetics or a detailed chemical reaction mechanism for hydrogen-oxygen-diluent mixtures. We also perform a large activation energy limit analysis, but the key new aspect in the asymptotic analysis is a particular distinguished limit, in which curvature effects are large enough to interact nontrivially with the highly sensitive ignition chemistry in the induction zone. It is this interaction which introduced the nonlinearity of the $D(\kappa)$ relation. A limiting curvature is found in both cases and the $D(\kappa)$ relationship is found to be multivalued. Previous studies[17] of related quasi-one dimensional detonation structure have found a similar multivalued solution. We compare the features of the solutions for detailed kinetics with the results of the asymptotic analysis and find useful insights. Some speculations about the significance of the critical curvature to gaseous detonation phenomenology are given.

II. QUASI-STEADY, QUASI-ONE DIMENSIONAL REACTION ZONES

Consider a portion of a curved detonation wave with a local radius of curvature R and a characteristic thickness Δ, as shown in Fig. 2. For both propagating and stationary waves, it is possible to show that the reaction zone structure can be described by a simple set of ordinary differential equations if: a) the reaction zone is thin, $R \gg \Delta$; and, b) the characteristic time scale for the change in the shock speed is much longer than the passage time of fluid elements through the reaction zone, $\tau = \Delta/w \ll D/(\mathrm{d}D/\mathrm{d}t)$. These equations are simply the conservation laws of quasi-one-dimensional gas dynamics with area change and chemical reaction. They are the logical extension of the standard ZND model[2] for planar waves.

In a reference frame attached to the shock wave moving with velocity $D(t) = dR/dt$ into stationary reactants, see Fig. 2, the transformed distance and velocity variables are

$$\begin{aligned} x &= R(t) - r \\ w &= D(t) - u \end{aligned} \tag{1}$$

and the equations of motion are

$$\begin{aligned} \frac{\mathrm{d}}{\mathrm{d}x}(\rho w) &= -\rho w \frac{1}{A}\frac{\mathrm{d}A}{\mathrm{d}x} \\ \rho w \frac{\mathrm{d}w}{\mathrm{d}x} &= -\frac{\mathrm{d}P}{\mathrm{d}x} \\ \frac{\mathrm{d}}{\mathrm{d}x}(h + \frac{w^2}{2}) &= 0 \\ w\frac{\mathrm{d}y_k}{\mathrm{d}x} &= \frac{W_k \dot{\omega}_k}{\rho} \qquad (k = 1, \ldots, K) \end{aligned} \tag{2}$$

where the net molar rate of creation of species k has been denoted $\dot{\omega}_k$, which can be computed once a chemical reaction mechanism and set of reaction rates for the K species have been specified. Other symbols are: y_k, mass fraction of species k; W_k, molar mass of species k; ρ, mass density; h, specific enthalpy; P, pressure.

The stream tube area change $\mathrm{d}A/\mathrm{d}x$ is determined from the expression for the logarithmic derivative that is obtained from the small-curvature, quasi-steady limit (see Bdzil and Stewart[9] and the discussion in the Appendix)

$$\alpha = \frac{1}{A}\frac{\mathrm{d}A}{\mathrm{d}x} = \kappa(\frac{D}{w} - 1) \tag{3}$$

where κ is the curvature of the wave front

$$\kappa = \begin{cases} \dfrac{2}{R} & \text{spherical waves} \\ \dfrac{1}{R} & \text{cylindrical waves} \end{cases} \tag{4}$$

Note that this implies that the stream tube area $A(x)$ increases with downstream distance just behind the shock front.

A more convenient form[2] for computation is

$$\begin{aligned} \frac{\mathrm{d}P}{\mathrm{d}t} &= -\rho w^2 \frac{(\dot\sigma - w\alpha)}{\eta} \\ \frac{\mathrm{d}\rho}{\mathrm{d}t} &= -\rho \frac{(\dot\sigma - wM^2\alpha)}{\eta} \\ \frac{\mathrm{d}w}{\mathrm{d}t} &= w\frac{(\dot\sigma - w\alpha)}{\eta} \\ \frac{\mathrm{d}y_k}{\mathrm{d}t} &= \frac{W_k\dot\omega_k}{\rho} \qquad (k = 1, \ldots, K) \end{aligned} \tag{5}$$

in which the *thermicity* parameter $\dot\sigma$ has been used to denote the nondimensional chemical energy release rate.

$$\dot\sigma = \sum_{k=1}^{K} \left(\frac{W}{W_k} - \frac{h_k}{c_pT}\right)\frac{\mathrm{d}y_k}{\mathrm{d}t}$$

where W is the mean molar mass of the mixture, c_p is the mixture specific heat at constant pressure, and h_k is the specific enthalpy of species k. The sonic parameter η is defined using the Mach number M of the flow relative to the shock wave

$$\eta = 1 - M^2 \qquad M = \frac{w}{c}$$

A key issue is the boundary conditions for these equations. The flow properties at the beginning of the reaction zone are those computed from the shock jump conditions evaluated at fixed composition.

$$\rho_1 w_1 = \rho_2 w_2$$

$$P_1 + \rho_1 w_1^2 = P_2 + \rho_2 w_2^2 \tag{6}$$

$$h_1 + \frac{1}{2} w_1^2 = h_2 + \frac{1}{2} w_2^2$$

In these equations, states 1 are the reactant conditions upstream of the shock and $w_1 = D$. States 2 are those just downstream of the shock, or the von Neumann (vN) conditions, at the beginning of the reaction zone. In general, these equations must be numerically solved for state 2, given state 1 and D. In the analytical solution discussed subsequently, the strong shock approximate solution to these equations is employed.

Downstream, the flow must be nonsingular and eventually becomes supersonic in the wave frame. Since the flow starts off just behind the shock as subsonic, the sonic parameter η must pass through zero within the reaction zone. Inspection of the structure equations indicates that the only way in which this can occur and still have a nonsingular solution is for the numerator $\dot{\sigma} - \alpha w$ to vanish at the same time as η, i.e., at the sonic point $M = 1$. This will occur only for particular values of the shock velocity D_s for each value of the curvature κ. The appearance of a sonic point in this flow can be attributed to the competing effects of chemical energy release $\dot{\sigma}$ and area change $-w\alpha$ creating an effective *throat* or *converging-diverging nozzle* in the flow. The area function is actually monotonically increasing, $dA/dx > 0$, and tends to decelerate the initially subsonic flow behind the shock, driving it away from the sonic point. The thermicity $\dot{\sigma} > 0$ is positive in the main energy release region of the reaction zone and tends to accelerate the flow,

driving it toward the sonic point. The appearance of a sonic point at other than a physical area minimum and the eigenvalue nature of the flow is well-known in the context of the ideal dissociating gas[18] through a nozzle.

We conclude that we have a two-point boundary value problem with a regularity condition at one endpoint that determines the eigenvalue solutions $D(\kappa)$. For general reaction mechanisms and realistic thermodynamics, this problem will have to be solved numerically. In the following section, we show that it is possible to obtain an analytical solution for a perfect gas with a one-step irreversible reaction described by a first-order Arrhenius rate law with a large activation energy. Numerical solutions for this problem have also been obtained by a simple shooting procedure and the results are described in a later section.

III. NONLINEAR D-κ RELATION FOR LARGE ACTIVATION ENERGY

A common model used to examine issues in combustion modeling is a one-step, Arrhenius reaction with a perfect gas equation of state. The reactants and the products are assumed to have the same molar mass and the reaction is assumed to be first order. The reaction progress variable is λ, $\lambda = 0$ for pure reactant and λ =1 for pure product. The model reaction rate equation is of the form

$$\frac{\mathrm{d}\lambda}{\mathrm{d}t} = \dot{r}(\lambda, T)$$

The enthalpy of the reactant-product mixture is

$$h = c_p T - \lambda q$$

where q is the heat of reaction and c_p is the specific heat $c_p = \gamma R/(\gamma - 1) =$ constant. In this approximation, the reaction structure equations reduce to a single ordinary differential equation

$$\frac{\mathrm{d}u^2}{\mathrm{d}\lambda} = \frac{2(c^2\sigma)u^2}{c^2 - u^2}\left(1 - \frac{\kappa c^2(u + D)}{(c^2\sigma)\dot{r}}\right) \tag{7}$$

for the particle velocity, $u = -w$, in a lead-shock attached frame as a function of the reaction progress variable, λ, which varies from $\lambda = 0$ in the unburnt gases to $\lambda = 1$ in the burnt gas.[2,9,14] In Eq. (7), c is the local speed of sound, related to u by the energy equation (the third expression of Eq. 6), which for an ideal gas with constant ratio of specific heats, γ, becomes

$$c^2 = \frac{\gamma - 1}{2}\left(D^2 - u^2 + \frac{D_{\mathrm{CJ}}^2}{\gamma^2 - 1}\lambda\right). \tag{8}$$

The quantity $c^2\sigma$ is a constant in the model considered here and proportional to the chemical energy q per unit gas mass: $c^2\sigma = (\gamma - 1)\, q$ ($\sigma\dot{r} = \dot{\sigma}$ of the previous section). D

is the actual detonation speed, assumed to be close to the Chapman-Jouguet speed $D_{\rm CJ}$ and κ is the lead shock curvature which is assumed to be small compared to the inverse of a characteristic reaction zone thickness, Δ.

The detonation structure has to satisfy the lead shock jump conditions at $\lambda = 0$. In the strong shock approximation, these read

$$\left.\begin{aligned} c^2 &= \frac{2\gamma(\gamma-1)}{(\gamma+1)^2} D^2 \\ u^2 &= \left(\frac{\gamma-1}{\gamma+1}\right)^2 D^2 \end{aligned}\right\} \quad \text{at} \quad (\lambda = 0)\,. \tag{9}$$

In addition, the solution must satisfy the generalized CJ-condition

$$(c^2 - u^2 = 0) \quad \Leftrightarrow \quad \frac{\kappa c^2 (u+D)}{c^2 \sigma \dot{r}} = 1\,, \tag{10}$$

to allow passage through the critical sonic point $c^2 - u^2 = 0$. Equations (7)–(10) pose an Eigenvalue-problem for the detonation speed D, given a reaction rate law and the front curvature, κ. Here we consider a one-step irreversible Arrhenius reaction,

$$\dot{r} = (1-\lambda) B \exp\left(-\frac{E_a}{RT}\right)$$

where E_a is the activation energy, R the gas constant and $T = c^2/\gamma R$ the temperature. We assume a large activation energy, such that

$$\theta = \frac{\gamma E_a}{(c^2_{\rm vN})^{(0)}} \gg 1\,.$$

In this limit we expect the detonation speed eigenvalue to have an expansion

$$\frac{D}{D_{\rm CJ}} = (1 + \theta^{-1} d^*(\kappa^*, \gamma))$$

where $\kappa^* = \kappa/\kappa_{\rm ref}$ is a suitably scaled nondimensional curvature. We will define the reference curvature later in the analysis by the requirement that for $\kappa^* = 1$ the reaction / curvature term in Eq. (7) equals unity at post-shock conditions in the induction zone.

The solution strategy is as follows: First we analyze the induction zone by a perturbation expansion about von Neumann conditions of a plane wave. The induction zone solution diverges towards the main reaction region and in a next step we a derive separate main reaction layer solution, including a first order perturbation analysis **and** a discussion of the generalized CJ-condition. We finally match the induction and main reaction layer solutions and in this process find the desired D(κ) relation.

A. INDUCTION ZONE ANALYSIS

For the induction zone analysis it is convenient to solve for the temperature, or c^2, instead of the velocity u. Combining Eqs. (7) and (8) we find

$$\frac{{\rm d}c^2}{{\rm d}\lambda} = -\frac{\gamma-1}{2}\frac{{\rm d}u^2}{{\rm d}\lambda} + \frac{D_{\rm CJ}^2}{2(\gamma+1)}\,. \tag{11}$$

Next we expand the solution as

$$\begin{aligned} D &= D_{\rm CJ}(1+\theta^{-1}d^*) \\ \lambda &= \theta^{-1}\Lambda \\ c^2 &= (c^2)^{(0)}_{\rm vN}(1+\theta^{-1}C(\Lambda))\,, \end{aligned} \tag{12}$$

and we introduce a reference curvature $\kappa_{\rm ref}$ such that

$$\kappa_{\rm ref}\,\frac{\left[c^2(u+D)\right]^{(0)}_{\rm vN}}{(c^2\sigma\dot{r})^{(0)}_{\rm vN}} = 1\,.$$

Defining $\kappa^* = \kappa/\kappa_{\rm ref}$ and inserting the ansatz from (12) in (11) we find, after some lengthy calculations that

$$\frac{{\rm d}C}{{\rm d}\Lambda} = \alpha + \beta\kappa^* e^{-C(\Lambda)}\,, \tag{13}$$

where

$$\alpha = \frac{1}{(c^2_{\rm vN})^{(0)}} \left(\frac{D^2_{\rm CJ}}{2(\gamma+1)} - 2\frac{\gamma-1}{2} \left[\frac{c^2\sigma u^2}{c^2-u^2} \right]^{(0)}_{\rm vN} \right)$$

and

$$\beta = 2\frac{\gamma-1}{2} \left(\frac{c^2\sigma u^2}{c^2(c^2-u^2)} \right)^{(0)}_{\rm vN} .$$

Equivalently with the present ideal gas equation of state,

$$\alpha = \alpha(\gamma) = \frac{3-\gamma}{4(\gamma-1)} , \qquad \beta = \beta(\gamma) = \frac{\gamma-1}{4\gamma} .$$

An initial condition for (13) is obtained by expanding the lead shock jump conditions (9). We find that

$$C(0) = 2d^* . \tag{14}$$

and the exact solution to Eq. (13) is

$$C(\Lambda) = \ln \left[(e^{2d^*} + \frac{\beta}{\alpha}\kappa^*)e^{\alpha\Lambda} - \frac{\beta}{\alpha}\kappa^* \right] . \tag{15}$$

Obviously, $C(\Lambda)$ diverges as $\Lambda \to \infty$ and one has to match the induction zone solution to the main reaction zone where $c^2 - (c^2_{\rm vN})^{(0)} = O(1)$.

B.THE MAIN INDUCTION REGION

The key observation here is that the curvature-reaction rate ratio (the last term in Eq. 7) becomes **exponentially** small as soon as $O(1)$ deviations of the temperature from post-shock conditions occur. Therefore one has

$$\left(\frac{{\rm d}c^2}{{\rm d}\lambda} \right)_{\rm MRL} = \frac{D^2_{\rm CJ}}{2(\gamma+1)} - 2\frac{\gamma-1}{2}\frac{(c^2\sigma)u^2}{c^2-u^2} + \quad \text{exp. small terms} , \tag{16}$$

and the main reaction zone has a plane wave structure except for exponential corrections. The correct initial condition for (16) is derived from the **generalized CJ-condition**:

As the solution passes through the critical point, the curvature-reaction rate ratio term in Eq. (7) must approach unity. Due to the exponentially large rate coefficient this can happen only for $(1-\lambda)$ being exponentially small. One can see this more clearly by writing

$$\kappa \, \frac{c^2(u+D)}{c^2 \sigma \dot{r}} = \kappa^* \quad \frac{c^2(u+D)}{[c^2(u+d)]^{(0)}_{\rm vN}} \quad \frac{1}{1-\lambda} \exp\left(\theta \left[\frac{c^{2\,(0)}_{\rm vN}}{c^2} - 1\right]\right)$$

and observing that κ^* and the second factor on the right hand side are O(1), so that the last term, too, must be O(1) and hence $(1-\lambda)$ must be exponentially small.

On the other hand one can show that the slope $dc^2/d\lambda$ in the c^2-λ-plane remains of order $O(1)$ throughout on the correct path that passes through the critical point. As a consequence, the solution must be exponentially close to sonic conditions when the thin transonic region where curvature and reaction effects can again compete is entered.

It follows that the correct boundary condition for (16) to all orders in θ^{-1} is:

$$(c^2 - u^2) = 0 \quad \text{at} \quad \lambda = 1\,. \tag{17}$$

Together with (8) this gives a value for c^2 or u^2.

The solution in the main reaction layer will be computed here for convenience in terms of the velocity

$$u = \left(-\frac{\gamma - \ell}{\gamma + 1} + \theta^{-1} U'(\ell)\right) D_{\rm CJ}\,,$$

where

$$\ell = \sqrt{1-\lambda}\,,$$

and where the leading term corresponds to the plane wave ZND- CJ-solution.[14] We use u instead of c^2, because it turns out that the first order perturbation of the velocity in the main reaction region is almost trivial and easy to compute.

The first order perturbation $U'(\ell)$ satisfies the equation

$$\frac{\mathrm{d}U'}{\mathrm{d}\ell} + \frac{\gamma}{\ell(\gamma-\ell)}U' = -\frac{\gamma-1}{\ell(\gamma-\ell)}d^* \,.$$

The generalized CJ-condition (17), together with (8) yields

$$U'(0) = -\frac{\gamma-1}{\gamma}d^* \,,$$

and the exact solution is

$$U' \equiv -\frac{\gamma-1}{\gamma}d^* = \mathrm{const}\,. \tag{18}$$

In the next subsection we match the induction zone solution (15) to the present solution (18) of the main reaction layer and obtain the desired $D(\kappa)$ relation.

C. MATCHING AND THE $D(\kappa)$ RELATION

We have to connect the main reaction layer solution for

$$\ell = 1 - \theta^{-1}\frac{\Lambda}{2} + \cdots \quad \to \quad 1\,,$$

i.e.

$$\left.\frac{u}{D_{\mathrm{CJ}}}\right|_{\mathrm{MRL}} = -\frac{\gamma-1}{\gamma+1} - \theta^{-1}\left(\frac{\Lambda}{2(\gamma+1)} + \frac{\gamma-1}{\gamma}d^*\right) + O(\theta^{-2}) \tag{19}$$

to the induction zone solution for $\Lambda \to \infty$. In Sec. III.A we derived the induction zone solution in terms of the dimensionless c^2-perturbation $C(\Lambda)$. Using (8) we can translate this result into an expression for the velocity perturbation $\tilde{U}$ defined by

$$\left.\frac{u}{D_{\mathrm{CJ}}}\right|_{\mathrm{ind}} = -\frac{\gamma-1}{\gamma+1} + \theta^{-1}\tilde{U}(\Lambda) + \cdots \,. \tag{20}$$

The large-Λ representation for $\tilde{U}$ becomes

$$\tilde{U}(\Lambda)\big|_{\Lambda\to\infty} \equiv -\frac{\Lambda}{2(\gamma+1)} + \frac{2\gamma}{\gamma^2-1}\ln\left(e^{2d^*} + \frac{\beta}{\alpha}\kappa^*\right) - \frac{\gamma+1}{\gamma-1}d^*\,. \tag{21}$$

Comparison of Eqs. (20) and (21) with (19) yields the matching condition

$$-\frac{\gamma-1}{\gamma}d^* = \frac{2\gamma}{\gamma^2-1}\ln\left(e^{2d^*} + \frac{\beta}{\alpha}\kappa^*\right) - \frac{\gamma+1}{\gamma-1}d^*\,,$$

which we rewrite in a more lucid form as

$$e^{\chi d^*} - e^{2d^*} = \tilde{\beta}\kappa^*\,. \tag{22}$$

Here

$$\chi(\gamma) = \frac{(\gamma+1)(3\gamma-1)}{2\gamma^2}\,,$$
$$\tilde{\beta}(\gamma) = \frac{\beta}{\alpha}(\gamma) = \frac{(\gamma-1)^2}{\gamma(3-\gamma)}\,.$$

Figure 3 shows the resulting double-branched curve in a d^* vs. κ^* diagram. The upper branch of the curve corresponds to the continuous extension of the plane Chapman- Jouguet detonation.

A quasi-steady solution of this type fails to exist once the scaled curvature exceeds

$$\kappa^*_{\max} = \left(\frac{\chi}{2}\right)^{\frac{\chi}{2-\chi}}\left(\frac{2-\chi}{2\tilde{\beta}}\right)\,.$$

At this point, the detonation speed defect is

$$d^*_{\max} = -\frac{\ln\frac{2}{\chi}}{2-\chi}\,.$$

The value of the quantities $\kappa^*_{\max}$ and $d^*_{\max}$ depends only on the ratio of specific heats γ. Numerical evaluation of these functions indicate that for realistic values, $5/3 \geq \gamma \geq 1$,

the detonation speed defect $d^*_{\max} \approx -0.50$, essentially independent of γ. The maximum curvature $\kappa^*_{\max}$ varies by a factor of two over this same range, $0.0758 \le \kappa^*_{\max} \le 0.1839$.

To compare these results to numerical solutions, we use the reaction zone length $\Delta_\circ = \Delta(\kappa = 0)$ rather than $\kappa_{\rm ref}$ as the scaling parameter. In the limit of large activation energy, the reaction zone length practically coincides with the induction length and, using the strong shock assumption, this length can be estimated to be

$$\Delta_\circ = \frac{4(\gamma-1)^2}{(\gamma+1)(3-\gamma)} \frac{D_{\rm CJ} e^\theta}{B\theta} \,.$$

Then the reference curvature can be written as

$$\kappa_{\rm ref} = \frac{A(\gamma)}{\theta \Delta_\circ} \qquad A(\gamma) = \frac{(\gamma^2-1)}{2\gamma(3-\gamma)} \tag{23}$$

and we find that the critical parameters can be written as

$$\begin{aligned} \frac{D_{\max}}{D_{\rm CJ}} &\approx 1 - \frac{1}{2\theta} \\ \kappa_{\max} &= \frac{\phi(\gamma)}{\Delta_\circ \theta} \end{aligned} \tag{24}$$

where $\phi = \kappa^*_{\max} A(\gamma)$. For small values of $\gamma - 1$, the function $\phi \sim (\gamma-1)/4e + O(\gamma-1)^2$ and the maximum value of $\phi = 0.030$ for $\gamma = 5/3$. The scaling with $\Delta_\circ$ and the dependence of $D_{\max}$ on θ is observed in the numerical simulations for H_2-O_2-diluent mixtures, as discussed subsequently.

Comparison to the previous work of Klein and Stewart[14] is possible for small values of $\Delta_\circ \kappa$ and large values of θ. Expansion of the results obtained in the present computation yields

$$\frac{D}{D_{\rm CJ}} \sim 1 - \frac{4\gamma^2}{\gamma^2-1} \Delta_\circ \kappa \,. \tag{25}$$

Correcting an algebra error in Klein and Stewart, we find an identical expression for large θ. Referring to Klein and Stewart, this requires taking the limit as z^* vanishes in their Eq. (75) and evaluating their Eq. (68) for large θ. This form of the $D(\kappa)$ relation is also confirmed by the numerical studies on H_2-O_2-diluent detonations, as described subsequently.

The authors are aware of recent independent work of Yao and Stewart[15] that has led them to the same nonlinear curvature-detonation speed relation in the limit of large activation energy that we discussed in this section. An ad hoc analysis of the same problem by He and Clavin[16] has also been recently independently carried out. Their analysis yields qualitatively similar results, although it is not based on activation energy asymptotics, but rather on the square wave model for the detonation structure.

IV. NUMERICAL SOLUTIONS

The full reaction zone equations (5) and jump conditions (6) have been numerically solved to obtain solutions $D(\kappa)$ for H_2-O_2-diluent mixtures. A detailed chemical reaction mechanism[19] and realistic thermochemistry[20] have been used in these computations. The solution procedure used was the standard method of "shooting" for determining the correct value of D for a given value of κ. First, an initial guess for the detonation velocity was determined by carrying out a standard CJ calculation. Second, an estimate for the critical curvature was obtained using the reaction zone length $\Delta_{\rm CJ}$ and the asymptotic result (23) with an estimated value of θ. A series of computations were then carried out for curvatures between zero and the estimated maximum value.

For each curvature and putative value of D, the jump conditions (6) were solved using the root finder ZEROIN[21] to obtain the initial conditions (vN point) for the reaction zone structure equations. Then a stiff solver based on Hindmarsh's LSODE package[22] and CHEMKIN[23] was used to integrate from the vN point toward the sonic point. A corrected value of the detonation velocity D was then estimated based on the outcome of this computation. This correction was based on wether the endpoint was sonic or subsonic. The distinction between the two types of solutions was made by simply observing the behavior of the Mach number during the integration. Solutions with a sonic endpoint have Mach numbers that monotonically increase toward one near the end of the computation. Solutions with a subsonic endpoint exhibit a maximum of the Mach number (< 1), then the Mach number approaches zero at a finite location downstream. By bracketing the location of the change between sonic and subsonic termination to a specified degree of accuracy,

an approximation (good to within 0.5 m/s) to the eigenvalue $D(\kappa)$ was obtained. In the vicinity of the critical curvature $\kappa_{\max}$, the iteration is most readily carried out with κ using fixed values of D. Just as in the asymptotic analysis, a double-valued $D(\kappa)$ function was obtained with both upper and lower branches. The solution for 30% hydrogen in air is shown in Fig. 4.

A. THE ZERO-CURVATURE EIGENVALUE SOLUTION

Surprisingly, in some cases with $\kappa = 0$, a sonic point was found in our numerical solution of the reaction zone problem. This results in an eigenvalue solution $D(0)$ which is different from the usual CJ velocity. The possibility of this has been known for some time and is extensively discussed in Fickett and Davis. However, aside from some speculations[24,25] about exotic chemical systems such as the H_2-Cl_2 reaction, the appearance of this feature in a common system such as hydrogen-air has not been previously documented. It is worthwhile to explore this feature of the solution since it is a rather subtle effect.

The standard introductory textbook presentations on detonation determine the minimum detonation velocity for the $\kappa = 0$ case from the jump conditions, considering the downstream state to be in equilibrium. This minimum velocity obtained from the jump conditions is known as the Chapman-Jouguet (CJ) velocity. However, computations of the ZND reaction zone structure with realistic reaction mechanisms lead to eigenvalue solutions $D(0)$ that are sometimes slightly higher than $D_{\rm CJ}$. Only in the special situation that the reactions are irreversible and are all exothermic will the two velocities be equal. The reaction used in our large activation energy analysis is of this type.

The difference between the results of the two approaches to minimum detonation

velocity has been known since Zeldovich[26] but not widely appreciated in the general combustion literature. In fact, Zeldovich developed the reaction zone structure analysis as a mechanistic explanation of why a minimum detonation velocity was physically significant. The significance for practical applications is diminished due to all the other nonideal aspects of detonations such as instability, yielding confinement and boundary layer effects that create a substantial velocity deficit.

The difference between the usual CJ velocity and $D_s(0)$ can be understood in terms of the role of kinetics and reverse reactions in the approach to equilibrium at the end of the reaction zone. The computed spatial distributions of the flow variables, selected species and the thermicity parameter are shown in Figs. 5-8 for a stoichiometric hydrogen-air detonation ($\kappa = 0$). The branching chain reactions produce an exponential buildup of radicals H, O and OH during the induction period located from just behind the shock up to 0.2 mm. During this period the thermicity is very small, see Fig. 7. In the enlargement of Fig. 8, it is apparent that $\dot{\sigma}$ is initially slightly negative due to the endothermic dissociation processes at the start of the reaction.

At a distance of about 0.2 mm, a large positive excursion in the thermicity (see Fig. 7) occurs due to the recombination of radicals into water

$$\mathrm{H + OH + M \longrightarrow H_2O}$$

Following this excursion, there is a period of adjustment in which the transient high concentrations of radical species approach the equilibrium values. This process results in a gradual reduction of $\dot{\sigma}$ that produces the long tail seen in Fig. 7. The final stage in this equilibration process is a slower dissociation process that converts some of the water into

OH and H_2. This causes the thermicity to become slightly negative for the final portion of the reaction zone. The sonic point is indicated on Fig. 5 and occurs at the point where $\dot{\sigma} = 0$, at $x = 22.5$ mm. This effect is quite small in magnitude (see Fig. 8) but significant to the eigenvalue nature of the solution for κ. The effect is more pronounced for some mixtures than others, see Tables I to III.

Three aspects of these equilibration processes are significant for producing the eigenvalue nature of the solution a) multiple species b) endothermic reactions c) reversible reactions. As discussed in Fickett and Davis,[2] all of these lead to the possibility of an eigenvalue detonation. The key factor is the dissociation resulting in the negative $\dot{\sigma}$ at the very end of the reaction zone. This produces a location of zero thermicity in the reaction zone where a sonic point can exist. The enthalpy at the sonic point, which determines the wave speed, is larger than the equilibrium enthalpy at the end of the reaction zone and so the wave speed is higher. An alternative, but really equivalent, explanation can be given in terms of the difference between frozen and equilibrium sound speeds.

It is proven in all elementary texts on combustion that the CJ solution is equivalent to selecting the situation in which the flow velocity w is equal to the *equilibrium* sound speed c_e (computed with the species in equilibrium) at the end of the reaction zone. On the other hand, the detonation structure computation determines the minimum speed $D_s(0)$ as that state in which the flow velocity w is equal to the frozen sound speed $c_f = c$ (computed with a fixed composition) at the sonic point, the effective end of the reaction zone. For a realistic reaction mechanism containing reversible reactions, the frozen and the equilibrium sound speeds are unequal, with the frozen sound speed being slightly higher

than the equilibrium.[18] As a consequence the minimum speed $D(0)$ can be slightly higher (0.1 to 0.5%) than the CJ speed. See Klein[27] for a discussion of equilibrium effects in the structure of weakly curved detonations.

B. REACTION ZONE STRUCTURES FOR CURVED WAVES

As the curvature is increased, the reaction zone structure gradually changes. Since the critical value of curvature is quite small, the effect of curvature on the structure of the initial portion of the reaction zone is very modest. The reaction zone structures for three different curvatures are shown in Figs. 9-12. From these solutions is it clear that only a very small change in area occurs in the region between the shock $x = 0$ and the sonic point for values of κ comparable or less than the critical value $\kappa_{\max}$. Initially, since the thermicity is nearly zero just behind the shock, the flow is nearly isentropic and the area variation is approximately

$$A/A_\circ \sim 1 + \frac{2}{\gamma - 1}\kappa x + O(\kappa x)^2 \,.$$

The flow in this region is subsonic, so the velocity decreases while pressure, temperature and density increase with distance due to essentially isentropic compression in the diverging stream tube. These variations are barely observable trends in the induction region of Figs. 9-12. The extent of the induction region increases as the shock velocity decreases, for $\kappa = 0$, the induction region extends to about 0.15 mm, for $\kappa = 0.07$ mm^{-1}, .2 mm and for $\kappa = .1325$ mm^{-1}, 0.5 mm. This is due to the very strong dependence of the reaction rate on the post-shock temperature, which in turn depends on the shock velocity D.

The most prominent feature of these plots is the large increase in velocity, temperature and Mach number with distance and the decrease of pressure with distance as the chemical

energy is released into the flow. In those cases with $\kappa < \kappa_{\max}$, this results in the appearance of the sonic point in the flow. The location of the sonic point moves upstream, toward the shock, as the shock velocity decreases. For $\kappa = 0$, the sonic point is located at 22.5 mm; for $\kappa = 0.07$ mm^{-1}, at 4.0 mm; for $\kappa = 0.1325$ mm^{-1}, at 3.21 mm. The behavior downstream of the sonic point can be either subsonic or supersonic flow for κ less than $\kappa_{\max}$. Either situation can be simulated in numerical solutions by applying a small perturbation to the solution as it emerges from the sonic point. In Figs. 9 and 10, the supersonic solutions are shown, while Figs. 11 and 12 are the subsonic solutions.

Supersonic solutions downstream of the sonic point have similar features to the usual quasi-one-dimensional supersonic isentropic flow. Flow velocity, Mach number and area all increase with increasing distance and the pressure and temperature decrease. Due to the form of the area relationship, Eq. (3), the solution asymptotes to a constant state far downstream since $w \to D$. Subsonic solutions downstream of the sonic point also have similar features to the usual quasi-one-dimensional subsonic isentropic flow. Flow velocity and Mach number decrease with increasing distance and the pressure, temperature and area increase. The solution terminates with infinite area and zero velocity at a finite distance downstream, again due to the particular form of the area relationship, Eq. (3). Consideration of a flow for which the Mach number vanishes at a finite point $x = x_o$, reveals that the area must become singular according to the relation

$$\frac{A}{A^*} \sim \frac{c_o}{D} \frac{1}{\kappa(x_o - x)} .$$

This can be observed in Fig. 12, the computation of Fig. 11 was stopped before the singularity was approached.

The reaction zone structure obtained for $\kappa > \kappa_{\max}$ is very similar to that for $\kappa < \kappa_{\max}$, as shown in Fig. 12, except there is no sonic point. It is very important to recognize that the reaction is not quenched in such cases, but simply that it is not possible to obtain sonic flow and therefore the reaction zone is entirely subsonic. Energy release (thermicity) profiles for the four cases considered in the previous figures are shown in Fig. 13. Note that κ plays essentially no role except in the vicinity of the sonic point, which is far behind the point of maximum thermicity $\Delta_\circ$ in all cases. The differences in the initial portions of the reaction zone profiles can all be accounted for by the differences in the initial post-shock state. This is particularly apparent if the two curves representing $\dot{\sigma}$ for the $\kappa = 0.1325$ mm^{-1} and the $\kappa = 0.2656$ mm^{-1} cases are compared. These are identical up to the thermicity peak and only begin to differ appreciably after $x = 1$ mm.

C. SUMMARY OF NUMERICAL RESULTS

The $D(\kappa)$ relation computed for 30% hydrogen-air is compared to the results of the asymptotic analysis (Eq. 22) in Fig. 4. The parameter $\gamma = 1.318$ used in this comparison was computed from the thermodynamic properties of the shocked reactants and the parameter $\theta = 7.79$ was determined by a separate explosion time computation as described in Shepherd.[28] It is clear that the asymptotic analysis captures the essential physics of the problem despite the enormous simplification of the chemistry and thermodynamics.

To examine the quantitative usefulness of the asymptotic analysis, a series of computations have been carried out for a range of hydrogen concentrations between 10 and 60%. The results are given in Table I and have been shown in scaled form in Fig. 14 for the upper portion of the $D(\kappa)$ function only. The form of the scaling is suggested by

basic dimensional considerations and results of the asymptotic analysis given above. The D/D_{CJ} vs $\Delta_\circ\kappa$ curves all have a similar shape but there are systematic differences due to the variation of γ and θ for each mixture. Away from the endpoints, each curve is approximately linear, in agreement with Eq. (25). The variation in slopes is due to the variation of γ as a function of composition, see Table I.

There is a systematic variation of the detonation speed defect $(D - D_{\rm CJ})/D_{\rm CJ}$ at the critical curvature. Examination of the maximum defects as a function of hydrogen concentration reveals a nonmonotonic variation with concentration. The asymptotic analysis would ascribe this as due to differences in the nondimensional activation parameter θ for these systems (Eq. 23). The hydrogen-air system has been extensively studied and previous[28] computations of θ are available (Fig. 15 and Table I) to test this relationship. The unusual behavior of activation energy with hydrogen concentration has been noted previously[28] and is due to the competition between various reaction channels. As discussed subsequently, the asymptotic analysis adequately explains the systematic variations for the case of hydrogen-air mixtures except in the case of large argon dilution, discussed further below.

The $D(\kappa)$ relation was also computed for stoichiometric hydrogen-oxygen-diluent mixtures for diluents of nitrogen and argon. The maximum curvature as a function of dilution is given in Fig. 16 and Tables II and III. The maximum curvature decreases strongly with increasing nitrogen concentration but displays a shallow maximum for an argon concentration of 30%. The $D(\kappa)$ curves for the nitrogen-diluted cases are similar to those shown in Fig. 14. The argon dilution $D(\kappa)$ curves, shown in Fig. 17, are more unusual in that

there is a pronounced inflection point for the highly-diluted cases. In part, this is due to the thermodynamic variations that occur when argon is added. Despite the dilution of the mixture with increasing argon content, the specific heat of argon is lower than that of either the reactants or the major products. As a consequence, the shock CJ temperature increases with increasing argon dilution. This is why the parameter θ decreases with increasing argon concentration up until 70 % argon. On the other hand, the CJ post-shock temperature decreases monotonically with increasing nitrogen concentration.

The numerical predictions of the maximum velocity deficit and maximum curvature are compared with the asymptotic analysis in Fig. 18 for all cases. Except for the velocity deficits in the case of argon concentrations greater than 30%, the asymptotic analysis and the numerical shooting solutions are in good agreement. The unusual $D(\kappa)$ curves for mixtures diluted with argon may be related to the observations[29,30,31] on cellular structure regularity and critical tube diameter d_c. Mixtures containing large amounts of argon are observed to have very regular cellular structures and critical tube diameters that are 25 to 30 cell widths. This is in contrast to mixtures with air or nitrogen dilution which have irregular cellular structures and critical tube diameters of 10 to 13 cell widths. The failure of the asymptotic solution to correctly describe the numerically predicted values of $\kappa_{\max}$ may be another manifestation of the unusual nature of mixtures with large amounts of argon. The failure of argon-diluted mixtures to scale in the same fashion as the nitrogen-diluted mixtures indicates that it may not be just a matter of cellular regularity but an intrinsic thermochemical effect of these mixtures. A similar notion was expressed by Shepherd et al.[30] based on analyses of overdriven detonations.

V. SIGNIFICANCE TO DETONATION PHENOMENA

A key problem in detonation physics today is the computation of critical conditions[5] for detonation initiation and propagation. Previous efforts in this area have been largely based on ad hoc models and/or simple dimensional considerations. For example, there is a large body of work[28,32] that proposes correlations of parameters such as detonation cell width λ, initiation energy E_c and critical tube diameter d_c with $\Delta_{\rm CJ}$. While acknowledging the crude nature of these efforts, they have provided the most practical means of estimating detonation sensitivity from fundamental chemical considerations.

One of the principal results of these studies is the extreme disparity between the reaction zone length and the scales of the phenomena, indicative of the singular perturbation character of disturbances to reaction zones. Comparisons between measured[33,34] lengths λ, d_c and $R_c = (E_c/\rho_\circ U_{\rm CJ}^2)^{1/3}$ and the reaction zone length $\Delta_\circ$ are shown in Fig. 19 for hydrogen-air mixtures. For example, λ is typically between 30 and 90 times the reaction zone length $\Delta_{\rm CJ}$ ($\simeq \Delta_\circ$) and d_c is 200 to 300 times $\Delta_{\rm CJ}$. Similar comparisons[35] can be made for other combinations of fuel and oxidizer which lead to the same conclusions. Linear stability analyses[7] are totally inadequate to explain these large ratios, predicting instead ratios that are $O(1)$.

An additional major critique of this approach is based on the observation that detonation structures typically involve several distinct internal subzones in which different physical and chemical kinetic processes are active. In most gaseous systems one can identify, e.g., an induction zone, a zone of major exothermal recombination and a region of approach to equilibrium.[28,36] Each of these sublayers has its own characteristic spatial ex-

tension and the ratios of these lengths vary from one system to the next as well as with the unburnt gas conditions for a given fixed system. It follows that a unique identification of "*the reaction zone thickness*" is simply meaningless. In addition, assuming such a reaction length had been assigned, it remains unclear what physical connection would exist between this scale and the critical scales of detonation propagation.

The present computations provide values for the critical (minimum) radius of curvature for the establishment of a quasi-steady detonation. It is tempting to propose that these are proportional to the critical tube diameter d_c or the initiation radius R_c. Even though it is not clear how to make this correspondence rigorous, there are strong arguments suggesting that such a relation does exist and can be established by further pointed analyses. The critical radius of curvature is an integral length that defines a global geometrical failure scale for a given explosive system. Its definition is unique and, in particular, does not depend on the details of the reaction zone structure. In addition we will find below that the critical radii of curvature are of the same order of magnitude as the critical scales of detonation propagation, such as the detonation cell size or the critical tube diameter (see also He and Clavin[16]).

For gaseous mixtures, the instability of the reaction zone and the onset of transverse waves occur simultaneously with detonation initiation so that the value of one-dimensional analysis appears limited. However, we can demonstrate the plausibility of this notion by comparison of the computed critical curvatures with measured detonation parameters. For a spherical wave, the asymptotic analysis indicates that the minimum radius is

$$R_{\min} = \frac{2}{\kappa_{\max}} = \frac{2\Delta_\circ \theta}{\phi(\gamma)} \,.$$

For a typical fuel-air mixture, $\gamma \sim 1.15$, $\phi = 0.011$ and $\theta = 5$ so that $R_{\min} \sim 1000\Delta_\circ$! The present numerical computations for hydrogen-air give values between 400 and 1000 for this ratio. The minimum radius of curvature varies strongly with the hydrogen concentration (see Fig. 19) due to the strong dependence of the reaction zone length $\Delta_\circ$ on the equivalence ratio. As a scaling or reference length scale, the critical curvature is much more reasonable than the reaction zone length, as demonstrated by Fig. 19.

A. CRITICAL INITIATION ENERGY

He and Clavin[16] have carried this observation even farther and proposed that the quasi-steady analysis can be used to provide a quantitative estimate of the critical initiation energy E_c. Their reasoning is as follows: The initial phase of shock initiation in a spherical geometry is treated by using the strong shock similarity solution for the shock wave radius $R_s(t)$

$$R_s = \eta_o \left(\frac{E_c}{\rho_o}\right)^{1/5} t^{5/2}, \tag{26}$$

where η_o is a constant of $O(1)$ that is determined by the ratio of specific heats γ. Differentiation of this expression enables the shock velocity U_s to be expressed as a function of the shock radius R_s

$$U_s = \frac{2}{5}\eta_o^{5/2} \left(\frac{E_c}{\rho_o}\right)^{1/2} \frac{1}{R_s^{3/2}}. \tag{27}$$

Their key assumption is that a self-sustained detonation will be produced only if $R_s > R_{min}$ when the shock velocity falls below D_{min} where R_{min} and D_{min} are computed from the quasi-steady analysis.

This is illustrated in Fig. 20 by plotting the $D(\kappa)$ relation (22) obtained from the asymptotic analysis ($\theta = 15$) together with the blast decay relation (27). Shown are three

blast wave conditions, labeled supercritical, $E > E_c$; critical, $E = E_c$; subcritical, $E < E_c$. The critical conditions shown graphically in Fig. 20 yield the following estimate for the critical initiation energy

$$E_c = \rho_o U_{min}^2 \left(\frac{5}{2}\right)^2 \frac{1}{\eta_o^5} R_{min}^3 \,, \tag{28}$$

where R_{min} is given by (26) and $U_{min} \approx U_{\rm CJ}$ as follows from (24) for $\theta >> 1$. Therefore, the critical energy can be estimated as

$$E_c \approx A \rho_o U_{\rm CJ}^2 \Delta_o^3 \,,$$

where A is the combination of parameters

$$A = \theta^3 \left(\frac{5}{2}\right)^2 \frac{1}{\eta_o^5} \frac{2^3}{\phi^3} \,.$$

For a typical fuel-air mixture $\eta_o = 1.005$, $\phi = 0.011$. The effective activation energy θ is between 5 and 30 (Tables I to III) for these mixtures, resulting in a value of A between 5×10^9 and 1×10^{12}.

The results presented in Fig. 19 and Fig. 21 provide a quantitative evaluation of this idea. The estimate of (28) can be written as

$$R_{c,predicted} = 1.8 R_{min} \tag{29}$$

where $R_c = (E_c/\rho_\circ U_{\rm CJ}^2)^{1/3}$ is the initiation length scale. From the evaluation shown in Fig. 19, the computed values of R_{min} are actually larger than the experimental value of R_c. At stoichiometric, the ratio R_c/R_{min} is 0.7. The ratio decreases as the equivalence ratio either increases or decreases from 1, reaching a minimum value of about 0.2 at the extreme endpoints of the range shown in Fig. 19. This (29) implies that the critical energy will be overestimated by one to two orders of magnitude.

This idea is a variation of the original analysis of Zeldovich et al.[37] and the extension by Lee et al.[38] who both used similar considerations but based on minimum energy release or elapsed time rather than a minimum wave curvature. These ideas also result in a similar dependence of the initiation energy on the reaction zone parameters:

$$E_c = A' \rho_o U_{\mathrm{CJ}}^2 \Delta_o^3 \tag{30}$$

where A' is a constant of the order of 10^5. Those models typically underestimate the critical initiation energy by several orders of magnitude since the experimentally deduced value of A' is about 3×10^8.

Lee has proposed[5,34] an empirical correlation with the experimentally measured cell width λ replacing the reaction zone thickness Δ. The original form of his correlation was written in terms of the *blast scaling radius* $R_b = (E_c/P_\circ)^{1/3}$ but can also be written in terms of R_c as

$$E_c = A'' \rho_o U_{\mathrm{CJ}}^2 \lambda^3 \,,$$

where $A'' \approx 200$. This is consistent with (30) if the cell width is proportional to the reaction zone length with a constant of proportionality of about 100.

Comparison with the experimental data for H_2-Air mixtures is shown in Fig. 21 for the three different estimates for R_c discussed above. We find that the scaling length R_c can be approximated equally well by any of the following relationships:

$$R_c \approx 0.6 R_{min}$$

$$R_c \approx 6\lambda$$

$$R_c \approx 650\Delta$$

Inspection of Fig. 21 reveals systematic deviations from these simple estimates. Investigations with other fuel-oxidizer systems would be useful in understanding the nature of these deviations better. The results indicate that such estimates are useful but are often merely rough guides to the magnitude rather than precise relationships.

All of these ideas have an underlying assumption of quasi-steady behavior near the critical initiation condition. Detailed computations indicate that the time scales associated with the blast wave decay and quasi-steady evolution of slightly curved waves are incommensurate. Further, as discussed in the next section, the entire notion of quasi-steady behavior in high-activation systems is questionable.

We conclude that unsteadiness of the reaction zone is an essential component of establishing a detonation. An alternative model of the critical conditions for initiation can be developed[39] based on purely unsteady considerations. This can be made quantitative by analyzing the interaction of the reaction zone with the unsteady expansion wave following the blast wave. Computation of the time scales associated with this expansion indicates that they are of the order of the reaction time near the critical radius R_c. Competition between the chemical reaction and the quenching effects of the unsteady expansion can be used to define an alternative critical condition to (28). A realistic model must incorporate both the effects of unsteadiness and curvature.

VI. IS THE QUASI-STEADY ANALYSIS VALID?

What is the significance of the critical curvature and the large ratio between R_{min} and $\Delta_\circ$? Clearly, exceedingly small amounts of curvature result in the disappearance of sonic points *at the present level of approximation*. While it is tempting to conclude that this indicates failure of all but the most nearly planar waves, the numerical solutions for supercritical curvatures (see Fig. 12) clearly indicate that a strong exothermic reaction does occur in those cases while failure or quenching in the conventional sense does not.

A more logical conclusion is that the role of unsteadiness must be reconsidered in the analysis. Indeed, detonation waves in gases are overwhelmingly characterized by unsteadiness rather than quasi-steady behavior. It is clear that the quasi-steady approximation (see the Appendix) used to derive Eqs. (5) *fail* in the vicinity of the maximum curvature point. Less obvious is that for state-sensitive rates, unsteadiness appears to play an essential role even far from the critical region. The role of unsteady effects is considered briefly in the present section.

It is well known that the ZND detonation structure in the limit of large activation energy for one-step Arrhenius kinetics approaches a square profile. In this *square-wave* limit, the induction zone separating the lead shock and thermal explosion (fire) becomes extremely temperature sensitive. Stability analyses carried out in this limit[6,40] indicate catastrophic instability with unstable growth at arbitrarily high frequencies. Considering these results, one may well question the applicability of the quasi–steady, quasi–one–dimensional analysis of the present paper. We mention here two of the major issues related to this difficulty. The complete resolution of these issues is clearly a major research project

so we provide only a qualitative discussion of our proposed solutions and leave the resolution for future communications.

First, one may wonder whether the multitude of unstable modes present in the linear stability analysis would not destroy the quasi-steady wave structure on very short time scales. We notice, that

i) the catastrophic instability occurs in the limit of large activation energy, i.e., extreme temperature sensitivity of the induction length, and that

ii) the unstable eigenmodes refer to the *unperturbed* detonation structure, i.e., to a specific induction length of the square wave profile.

From i) it follows that a *very* small perturbation, of order $O(1/\theta)$, in shock strength will produce leading order changes of the induction time of fluid particles that have been processed by the shock. As a consequence, very small changes of the shock velocity will immediately cause the induction zone to shrink by a factor of order $O(1)$. Now assume that this change of the shock strength has been brought about by the growth of an unstable eigenmode. Then, due to the strong temperature sensitivity of the induction length and remark ii) above, this eigenmode will drive itself out of resonance and it will not grow any further.

Every unstable eigenmode that has a characteristic time comparable to the passage time of a particle through the detonation structure will suffer from this self-detuning mechanism and hence will most likely not be observed to grow to large amplitudes. In fact, numerical simulations of unstable one-dimensional detonations based on Arrhenius kinetics by Abouseif and Toong[41] or Bourlioux and Majda[42] show large amplitude nonlinear oscil-

lations with characteristic periods much longer than the above-mentioned passage time of a particle. i.e., the induction time. These results strongly support our qualitative arguments, and they might even find their explanation here. (See also Buckmaster,[43] Klein[44])

Second, the quasi–steady, quasi-one–dimensional analysis presented above assumes the fire to be at rest relative to the leading shock wave. This is explicitly used in the matching procedure in Sec. III.C. We will explain now that this assumption is valid only for strictly stationary flow configurations, but that the resulting $D(\kappa)$ relation cannot be used as an intrinsic front propagation law for evolving weakly curved waves.

Consider an evolving front with characteristic radius of curvature R, a typical induction length ℓ_I and front normal velocity of order $D_{\rm CJ}$. The characteristic evolution time scale for this wave will be

$$t_{\rm ref} = \frac{R}{D_{\rm CJ}} \tag{31}$$

and the wave front curvature will thus evolve on that time scale.

On the other hand, since we assume the distinguished limit

$$\theta \frac{\ell_I}{R} = O(1)$$

relating curvature and activation energy, these changes in the wave front curvature will produce leading order changes of the induction length. As a consequence, the fire moves relative to the lead shock at a speed

$$\dot{\ell}_I \sim \frac{\ell_I}{t_{\rm ref}} = \frac{1}{\theta}\, D_{\rm CJ}\,.$$

Hence, in the two frames of reference attached to the lead shock and the fire, the flow velocities will differ by order $O(1/\theta)$.

Next we recall that in the matching calculations of Sec. III.C, these first order velocities played a major role in determining the $D(\kappa)$ relation. It follows that the unsteady changes of the curvature, and hence of the induction length in an evolving front, will nontrivially modify the quasi-steady detonation speed-curvature relation (22) of this paper. Detailed computations[27] show that an inherently unsteady propagation law replaces the quasi-steady $D(\kappa)$ relation for large activation energy, provided the underlying assumption of a slow time scale evolution with the reference time scale from (31) takes place.

Despite the limited applicability of the present results, our analysis highlights the key effects of curvature in the presence of highly temperature sensitive induction kinetics. Further, it shows how to implement in this kind of analysis a detailed chemical kinetic reaction scheme and it has paved the way for further analyses including unsteady effects and large deviations from the CJ-speed.[27,44]

VII. CONCLUSIONS

We have presented numerical and approximate analytical solutions to the quasi-steady structure of curved detonation waves. Numerical solutions with a full thermochemical treatment are in reasonable agreement with the approximate large activation energy analysis except for mixtures with large amounts of argon dilution.

These solutions demonstrate the existence of a limiting critical curvature. For waves with a curvature larger than this maximum value it is not possible to find solutions that contain a sonic point. We propose two conclusions from these observations:

First, the critical radius of curvature appears to be an outstanding candidate for a characteristic length by which to scale the critical scales of detonation propagation, such as detonation cell sizes or critical tube diameters. It seems to be much better suited than a characteristic reaction zone thickness for this purpose, because it is (i) *uniquely* determined by the thermodynamic and chemical kinetic properties of the combustible and (ii) its order of magnitude matches that of the critical scales, while reaction length scales are typically a few orders of magnitude smaller.

Secondly, the significance of the failure of the quasi-steady theory for detonation propagation appears to be the onset of unsteadiness in the detonation process. Further analyses are needed, however, to establish this link in detail and to relate these effects to detonation quenching or failure.

APPENDIX: QUASI-STEADY REACTION ZONE EQUATIONS

For completeness, a simple derivation of the quasi-steady reaction zone equations is presented here. The validity of these equations is also examined in view of the approximate and numerical solutions that have been obtained in this paper. The key equation that has to be examined is conservation of mass

$$\frac{\partial \rho}{\partial t} + \nabla \cdot (\rho u) = 0 \tag{A.1}$$

Applying the transformations of Eq. (1), we obtain

$$\frac{1}{\rho}\left(\frac{\partial}{\partial t} + (D-u)\frac{\partial}{\partial x}\right)\rho = \frac{\partial u}{\partial x} - \alpha\frac{u}{R-x} \tag{A.2}$$

where $\alpha = 0$ (planar) or 1 (cylindrical) or 2 (spherical) depending on the geometry. The quasi-steady, slightly-curved approximate form of this equation can be deduced with the aid of the following order of magnitude estimates

$$x \sim \Delta\ ; \quad t_{\rm slow} \sim D/\frac{\partial D}{\partial t}\ ; \quad \tau \sim \frac{D-u}{\Delta}$$

Estimating the size of each term in Eq. (A.1), we find that in order to obtain the quasi-steady form of the equations we must have

$$t_{\rm slow} >> \tau \tag{A.3}$$

so that the evolution of the wave speed is slow compared to the transit time of fluid elements through the reaction zone. In the limit as $\tau/t_{\rm slow} \to 0$, the time derivative vanishes and we can treat R as a constant so that the equation effectively is time-independent. To further simplify the equation, we need to suppose that the reaction zone length is small

$$R >> \Delta$$

so that the last term in (A.2) can be expanded to yield the approximate expression

$$(D-u)\frac{\partial \rho}{\partial x} = \rho \frac{\partial u}{\partial x} - \frac{\alpha \rho}{R} u + O(\frac{x}{R})^2$$

which as $x/R \to 0$, yields the first equation of Eq. (2), taking into account the definition $w = D$ - u and Eqs. (3) and (4). Similar considerations (only involving the unsteady behavior) can be applied to the momentum, energy and species equations to obtain the results of Eq. (2).

The validity of the approximations can be *a posteriori* checked by using the solutions given in Secs. III and IV. For the regime of interest, the quantity $\Delta\kappa$ is of the order of 10^{-3} (see Fig. 14 and Eq. (24)), verifying that the slightly-curved approximation is valid. The time scale for the quasi-steady evolution of a spherical or cylindrical wave can be estimated by using the definition of curvature Eq. (4), the wave speed $D = \mathrm{d}R/\,\mathrm{d}t$ and the $D(\kappa)$ relation

$$\frac{\mathrm{d}D}{\mathrm{d}t} = -\frac{\kappa^2}{2} D \frac{\mathrm{d}D}{\mathrm{d}\kappa}\ ; \quad t_{\mathrm{slow}} = \frac{-2}{\kappa^2 \frac{\mathrm{d}D}{\mathrm{d}\kappa}}\ .$$

Clearly, as $\kappa \to \kappa_{\max}$, the derivative of the $D(\kappa)$ relation becomes infinite, the time scale t_{slow} will approach zero and the quasi-steady approximation will fail. Away from this point, i.e., for $\kappa < \kappa_{\max}$, the approximate relationship (25) can be used to show that the quasi-steady approximation is valid as long as (A.3) holds.

However, there are many situations in which there is an externally imposed evolution time scale. Examples are the situation discussed in Sec. V regarding the blast wave initiation and in Sec. VI regarding the role of instabilities. In these situations, the flow can no longer be quasi-steady since the detonation wave speed will be changing on a time scale comparable to or faster than the reaction time. This appears to be the case for many

physical problems of interest and is the motivation for considering an unsteady version of the $D(\kappa)$ relation, alluded to in Sec. VI.

REFERENCES

[1] W. W. Wood and J. G. Kirkwood, "The diameter effect in condensed explosives: The relation between velocity and the radius of curvature in the detonation wave," J. Chem. Phys. **22**, 1920 (1954).

[2] W. Fickett and W. C. Davis, *Detonation* (University of California Press, Berkeley, CA 1979).

[3] R. Klein, "On the Dynamics of Weakly Curved Detonations," in: *IMA-Volumes in Mathematics and its Applications* **35**, (Springer 1991).

[4] D. R. White, "Turbulent Structure of Detonation Waves," Phys. Fluids **4**, 465-480 (1961).

[5] J. H. S. Lee, "Dynamic Parameters of Gaseous Detonation," in *Ann. Rev. of Fluid Mech.* **16**, 311–336 (1984).

[6] J. J. Erpenbeck, "Theory of Detonation Stability," in *12th Symposium (Intl.) on Combustion* (The Combustion Institute, Pittsburgh, PA 1969), pp. 711–721.

[7] H. I. Lee and D. S. Stewart, "Calculations of linear detonation stability: One-dimensional instability of planar detonations," J. Fluid Mech. **216**, 103–132 (1990).

[8] A. Bourlioux and A. J. Majda, "Theoretical and Numerical Structure for Unstable Two-Dimensional Detonation," Combust. Flame **90**, 211–229 (1992).

[9] J. B. Bdzil and D. S. Stewart,"Modeling of two-dimensional detonations with detonation shock dynamics," Phys. Fluids **A1**, 1261 (1988).

[10] J. B. Bdzil, W. Fickett, and D. S. Stewart, "Detonation shock Dynamics: A new approach to modeling multi-dimensional detonation waves," in *9th Symposium (Intl.) on Detonation* (OCNR 113291–7, Washington, DC 1990), pp. 730–742.

[11] R. Engelke and J. B. Bdzil, "A study of the steady-state reaction zone structure of a homogeneous and heterogeneous explosive," Phys. Fluids **26**, 1210–1221 (1983).

[12] J. B. Bdzil and W. Fickett, "DSD Technology: A Detonation Reactive Huygens Code," Los Alamos Report LA–12235–MS, 1992.

[13] B. D. Lambourn and D. C. Swift, "Application of Whitham's Shock Dynamics Theory to the Propagation of Divergent Detonation Waves," *9th Symposium (Intl.) on Detonation* (OCNR 113291–7 1990), pp. 784–797.

[14] R. Klein and D. S. Stewart, "The relation between curvature, rate dependence and detonation velocity," SIAM J. Appl. Math **53**, 1401–1405 (1993).

[15] J. Yao and D. S. Stewart, "On the normal shock velocity-curvature relationship for materials with large activation energy," Combust. Flame **100**, 519-528 (1995).

[16] L.-T. He and P. Clavin, "On the direct initiation of Gaseous Detonations by an Energy Source," J. Fluid Mech. **277**, 227–248 (1994).

[17] S. Tsuge, "The effect of boundaries on the velocity deficit and the limit of gaseous detonations," Comb. Sci. Tech. **3**, 195–205 (1971).

[18] W. G. Vincenti and C. H. Kruger Jr., *Introduction to Physical Gas Dynamics* (McGraw-Hill, NY, NY, 1965).

[19] A. E. Lutz, R. J. Kee, J. A. Miller, H. A. Dwyer, and A. K. Oppenheim, "Dynamic Effects of Autoignition Centers for Hydrogen and $C_{1,2}$ Fuels," in *22nd Symp. (Int.) on Combust.* (The Combustion Institute, Pittsburgh, PA 1989) pp. 1683–1694.

[20] R. J. Kee, F. M. Rupley, and J. A. Miller, "Chemkin-II: A Fortran Chemical Kinetics Package for the Analysis of Gas-Phase Chemical Kinetics," Sandia National Laboratories Report SAND89-8009, 1989.

[21] L. F. Shampine and H. A. Watts, "ZEROIN, A Root-Solving Code," Sandia National Laboratories Report SAND SC-TM-70-631, 1970.

[22] A. C. Hindmarsh, "ODEPACK, A Systematized Collection of ODE Solvers," in *Scientific Computing* edited by R. S. Stepleman et al. (North-Holland, Amsterdam, 1983), pp. 55-64.

[23] R. J. Kee, F. M. Rupley, and J. A. Miller, "The Chemkin Thermodynamic Data Base," Sandia National Laboratories Report SAND87-8215, 1987.

[24] H. Guenoche, P. Le Diuzet, and C. Sedes, "Influence of the Heat Release Function on the detonation states," Prog. Astro. Aero. **75**, 387-407 (1981).

[25] R. Knystautas and J. H. S. Lee, "Detonation Parameters for the Hydrogen-Chlorine System," Prog. Astro. Aero. **114**, 32-44 (1988).

[26] Ya. B. Zeldovich, "On the Theory of the Propagation of Detonations in Gaseous Systems," JETP **10**, 542-568 (1940). Available in translation as NACA TM 1261 1950.

[27] R. Klein "Curved Detonations in Explosive Gas Mixtures with High Temperature Sensitivity," in preparation.

[28] J. E. Shepherd "Chemical Kinetics of Hydrogen-Air-Diluent Mixtures," Prog. Aero. Astro. **106**, 263-293 (1986).

[29] I. O. Moen, A. Sulmistras, G. O. Thomas, D. Bjerketvedt, and P. A. Thibault, "Influence of Cellular Regularity on the Behavior of Gaseous Detonations," Prog. Astro. Aero., **106**, 220-234 (1986).

[30] J. E. Shepherd, I. O. Moen, S. B. Murray, and P. A.Thibault, "Analyses of the Cellular Structure of Detonations," in *21st Symp. (Intl.) Comb.* (The Combustion Institute, Pittsburgh, PA, 1986), pp. 1649-1658.

[31] D. Desbordes, C. Guerraud, L. Hamada, and H. N. Presles, "Failure of the Classical Dynamic Parameters Relationships in Highly Regular Cellular Detonation Systems," Prog. Astro. Aero. **153**, 347-359 (1993).

[32] C. K. Westbrook and P. A. Urtiew, "Chemical Kinetic Prediction of Critical Parameters in Gaseous Detonations," in *19th Symposium (Intl.) on Combustion* (The Combustion Institute, Pittsburgh, PA 1982), pp. 615–623.

[33] C. M. Guirao, R. Knystautas, J. H S. .Lee, W. B. Benedick, and M. Berman, "Hydrogen-Air Detonations" in *19th Symposium (Intl.) on Combustion* (The Combustion Institute, Pittsburgh, PA 1982), pp. 583-590.

[34] W. B. Benedick, C. M. Guirao, R. Knystautas, and J. H. S. Lee, "Critical Charge for the Direct Initiation Detonation in Fuel-Air Mixtures," Prog. Astro. Aero. **106**, 181-202 (1986).

[35] J. E. Shepherd, "Detonation Waves and Propulsion," in *Combustion in High-Speed Flows*, Editors: J. Buckmaster, T. L. Jackson, and A. Kumar (Kluwer Academic Publishers 1994), pp. 373–420.

[36] A. E. Lutz, "A numerical study of autoignition," Sandia Report SAND88-8224, UC-4, 1988.

[37] Ya. B. Zeldovich, S. M. Kogarko, and N. N. Simonov, "An Experimental Investigation of Spherical Detonation of Gases," Soviet Physics - Technical Physics **1**, 1689-1713 (1956).

[38] J. H. S. Lee, B. H. K. Lee, and R. Knystautas, "Direct Initiation of Cylindrical Gaseous detonations," Phys. Fluids **9** , 221-222 (1966).

[39] J. E. Shepherd, "Direct Initiation of Detonation - A New Model,"presented at INRIA, "Nonlinear Applied Problems" sponsored by the CEA-EDF-INRIA, Roquencourt, FRANCE, May 14, 1993. (Unpublished)

[40] J. D. Buckmaster, "One-Dimensional Detonation Stability – The Spectrum for Infinite Activation Energy," Phys. Fluids **31**, 3571-3576 (1988).

[41] G.E. Abouseif and T.Y. Toong, "Theory of unstable one-dimensional detonations," Combust. Flame **45**, 67-94, (1982).

[42] A. Bourlioux and A. J. Majda, "Theoretical and Numerical Structure of Unstable Detonations," Phil. Trans. Roy. Soc. **A 350**, 29–68 (1995).

[43] J. D. Buckmaster, "Pressure Transients and the Genesis of Transverse Shocks in Unstable Detonations", Comb. Sci. & Technol. **61**, 1–20, (1988).

[44] R. Klein, "Analysis of Accelerating Detonation Using Large Activation Energy Asymptotics", in *Proceedings of 2nd Intl. Workshop on Microscopic and Macroscopic approaches to Detonation* (St. Malo, France, Oct. 1994) to appear in Les Editions de Physique, 1995.

TABLES

TABLE I. Hydrogen-Air Detonation Parameters

H_2	D_{CJ}	$D(0)$	$D(\kappa_{max})$	$\Delta_\circ$	θ	γ_{vN}	κ_{max}
%	(m/s)	(m/s)	(m/s)	(mm)			(mm^{-1})
10	1287.2	1289.3	1258.4	$5.232\times10^{+3}$	26.4	1.341	3.982×10^{-7}
15	1516.7	1523.8	1481.8	$3.210\times10^{+1}$	25.4	1.329	5.725×10^{-5}
20	1704.7	1715.4	1666.7	6.788×10^{-1}	22.0	1.323	1.450×10^{-3}
25	1860.7	1869.1	1763.9	2.398×10^{-1}	9.42	1.319	7.800×10^{-3}
30	1976.5	1984.6	1836.6	1.705×10^{-1}	7.79	1.318	1.327×10^{-2}
35	2050.7	2054.7	1910.2	1.736×10^{-1}	7.50	1.319	1.319×10^{-2}
40	2099.6	2101.2	1965.2	2.155×10^{-1}	8.57	1.322	9.710×10^{-3}
45	2140.9	2141.5	2030.4	2.999×10^{-1}	9.71	1.326	5.663×10^{-3}
50	2179.5	2179.5	2088.0	4.876×10^{-1}	13.0	1.330	2.625×10^{-3}
55	2216.1	2216.4	2133.9	$1.142\times10^{+0}$	21.8	1.336	9.915×10^{-4}
60	2250.7	2250.7	2168.1	$4.669\times10^{+0}$	25.8	1.342	3.390×10^{-4}
65	2282.7	2282.7	2205.3	$2.352\times10^{+1}$	22.7	1.348	9.687×10^{-5}
70	2311.4	2311.4	2236.0	$1.102\times10^{+2}$	22.0	1.356	2.055×10^{-5}

TABLE II. H_2-O_2-N_2 Detonation Parameters

N_2	D_{CJ}	$D(0)$	$D(\kappa_{max})$	$\Delta_\circ$	θ	γ_{vN}	κ_{max}
%	(m/s)	(m/s)	(m/s)	(mm)			(mm^{-1})
0	2842.2	2842.5	2589.2	4.230×10^{-2}	5.46	1.316	1.179×10^{-1}
10	2642.1	2648.2	2404.3	4.754×10^{-2}	5.58	1.316	9.940×10^{-2}
20	2473.6	2480.8	2263.3	5.513×10^{-2}	5.86	1.316	7.874×10^{-2}
30	2326.1	2333.5	2130.7	6.752×10^{-2}	6.18	1.315	5.818×10^{-2}
40	2186.9	2194.1	2009.8	8.818×10^{-2}	6.37	1.316	3.851×10^{-2}
50	2050.1	2056.7	1900.4	1.279×10^{-1}	7.09	1.317	2.102×10^{-2}
60	1904.8	1910.1	1790.5	2.336×10^{-1}	8.51	1.319	7.712×10^{-3}
70	1722.7	1724.9	1665.9	8.944×10^{-1}	17.2	1.324	8.255×10^{-4}
80	1468.5	1469.5	1425.9	$1.614\times10^{+1}$	24.1	1.334	1.190×10^{-5}

TABLE III. H_2-O_2-Ar Detonation Parameters

Ar	D_{CJ}	$D(0)$	$D(\kappa_{\max})$	$\Delta_\circ$	θ	γ_{vN}	$\kappa_{\max}$
%	(m/s)	(m/s)	(m/s)	(mm)			(mm^{-1})
0	2842.2	2842.5	2589.2	4.230×10^{-2}	5.46	1.316	1.179×10^{-1}
10	2565.5	2565.8	2301.3	3.790×10^{-2}	5.04	1.330	1.396×10^{-1}
20	2355.7	2355.9	2080.1	3.594×10^{-2}	4.40	1.348	1.528×10^{-1}
30	2189.6	2189.8	1904.7	3.573×10^{-2}	3.79	1.368	1.546×10^{-1}
40	2048.7	2048.7	1752.3	3.748×10^{-2}	4.06	1.392	1.450×10^{-1}
50	1925.1	1925.1	1622.9	4.190×10^{-2}	4.09	1.419	1.233×10^{-1}
60	1811.4	1811.2	1503.5	5.103×10^{-2}	3.91	1.452	9.202×10^{-2}
70	1693.8	1693.8	1377.1	7.223×10^{-2}	5.21	1.492	5.642×10^{-2}
80	1544.5	1545.1	1263.4	1.424×10^{-1}	5.41	1.540	2.240×10^{-2}

FIGURE CAPTIONS

FIG. 1. Examples of curved detonation fronts occurring in diffracting and propagating detonations. a) diffraction around a corner. b) yielding confinement. c) blast wave initiation. d) cellular instability.

FIG. 2. a) Spherical or cylindrical detonation front with a radius of curvature R. b) Equivalent quasi-one dimensional flow in the wave-fixed frame.

FIG. 3. Nondimensional solution d^* vs. κ^* for the large activation energy analysis.

FIG. 4. Detonation velocity D/D_{CJ} vs curvature κ for stoichiometric hydrogen-air at nominal initial conditions (298 K, 1 atm).

FIG. 5. Reaction zone structure for stoichiometric (30% H_2) hydrogen-air detonation with no curvature $\kappa = 0$, $D = 1984.6$ m/s. Normalized variables vs. distance downstream from shock. Nominal initial conditions (298 K, 1 atm). Sonic point at 22.5 mm, supersonic solution downstream.

FIG. 6. Reaction zone structure for stoichiometric (30% H_2) hydrogen-air detonation with no curvature $\kappa = 0$, $D = 1984.6$ m/s. Selected species mol fractions vs. distance downstream from shock. Nominal initial conditions (298 K, 1 atm).

FIG. 7. Reaction zone structure for stoichiometric (30% H_2) hydrogen-air detonation with no curvature $\kappa = 0$, $D = 1984.6$ m/s. Thermicity $\dot{\sigma}$ vs. distance from shock. Nominal initial conditions (298 K, 1 atm).

FIG. 8. Reaction zone structure for stoichiometric (30% H_2) hydrogen-air detonation with no curvature $\kappa = 0$, $D = 1984.6$ m/s. Thermicity $\dot{\sigma}$ vs. distance from shock. This is the

same data as Fig. 7 but with an enlargement of the ordinate showing the details of the endothermic regions. Nominal initial conditions (298 K, 1 atm).

FIG. 9. Reaction zone structure for 30% hydrogen-air detonation with a curvature about one-half the critical value $\kappa = 0.07075$ mm^{-1}, $D = 1917.03$ m/s. Sonic point at 4.00 mm, supersonic solution downstream. Nominal initial conditions (298 K, 1 atm).

FIG. 10. Reaction zone structure for 30% hydrogen-air detonation with a curvature near critical $\kappa = 0.1325$ mm^{-1}, $D = 1836.6$ m/s. Sonic point at 3.21 mm, supersonic solution downstream. Nominal initial conditions (298 K, 1 atm).

FIG. 11. Reaction zone structure for 30% hydrogen-air detonation with a curvature near critical $\kappa = 0.1325$ mm^{-1}, $D = 1836.6$ m/s. Subsonic solution downstream of sonic point. Nominal initial conditions (298 K, 1 atm).

FIG. 12. Reaction zone structure for 30% hydrogen-air detonation with supercritical curvature $\kappa = 0.2650$ mm^{-1}, $D = 1836.6$ m/s. Subsonic solution throughout. Nominal initial conditions (298 K, 1 atm).

FIG. 13. Thermicity vs. distance for the four 30% hydrogen-air detonation cases shown in Figs. 9-12.

FIG. 14. Detonation velocity D/D_{CJ} vs normalized curvature $\kappa\Delta_{\circ}$ for hydrogen-air mixtures between 10 and 60% hydrogen at nominal initial conditions (298 K, 1 atm). Only the upper portion of the $D(\kappa)$ function is shown.

FIG. 15. Nondimensional activation energy $\theta = E_a/RT_{\mathrm{vN}}$ for hydrogen-air mixtures at nominal initial conditions (298 K, 1 atm).

FIG. 16. Critical curvature vs. diluent concentration for H_2-O_2-diluent mixtures.

FIG. 17. Minimum detonation velocity D/D_{CJ} vs normalized curvature $\kappa\Delta_\circ$ for argon diluted stoichiometric hydrogen-oxygen mixtures. Nominal initial conditions (298 K, 1 atm).

FIG. 18. Comparison between the large activation energy (LAE) asymptotic analysis and numerical predictions. a) maximum velocity defect; b) maximum curvature.

FIG. 19. Minimum radius of curvature R_{min}, reaction zone length $\Delta_\circ$, cell width λ, critical tube diameter d_c, and critical initiation length scale $R_c = (E_c/\rho_\circ D_{\mathrm{CJ}}^2)^{1/3}$ as a function of hydrogen concentration for hydrogen-air mixtures at nominal initial conditions (298 K, 1 atm).

FIG. 20. Illustration of ideal self-similar blast wave decay vs. quasi-steady $D(\kappa)$ relation.

FIG. 21. Comparison of three estimates of critical initiation scaling length for the detonation of H_2-Air mixtures.

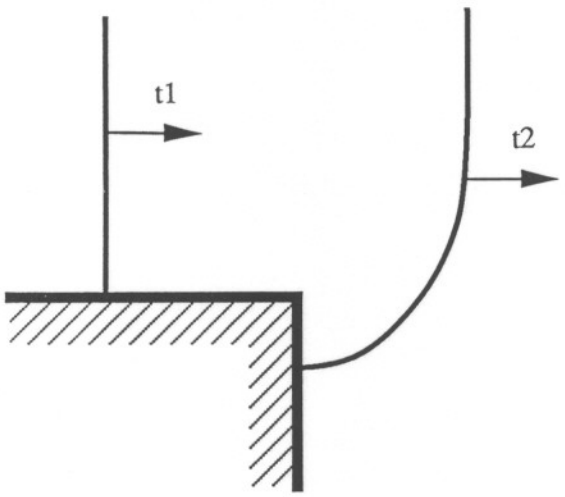

(a)

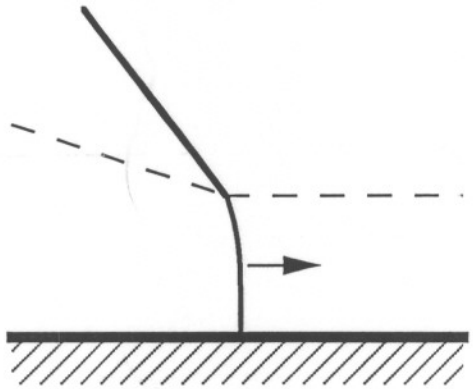

(b)

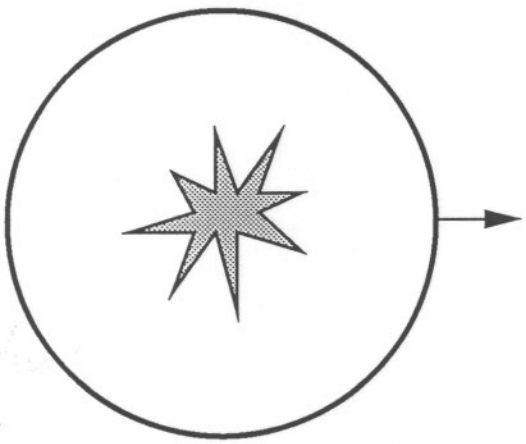

(c)

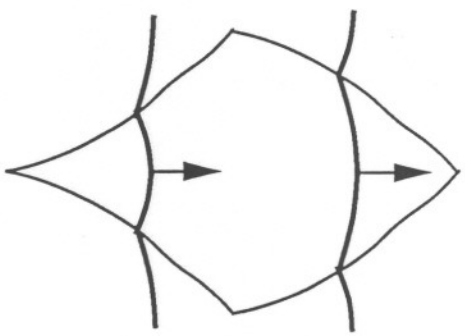

(d)

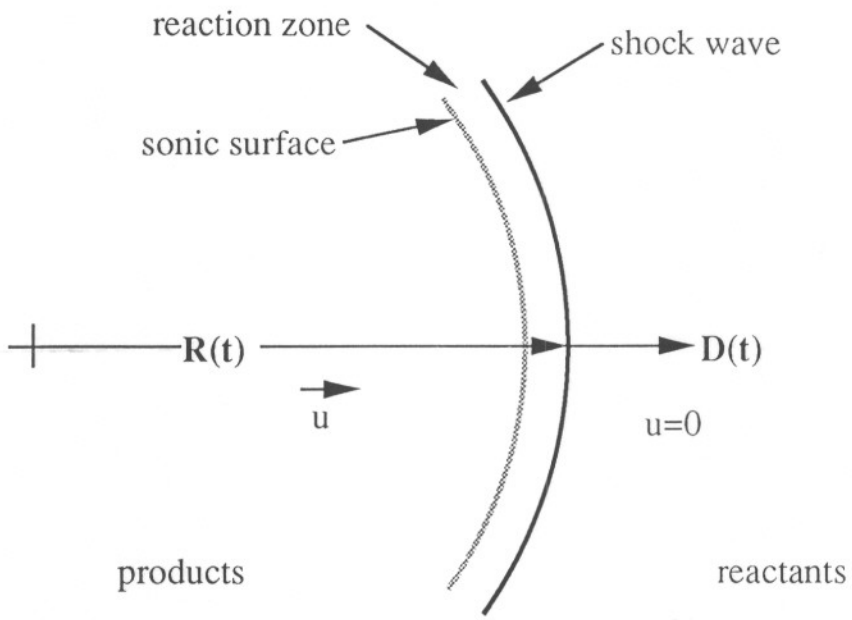
reaction zone
shock wave
sonic surface
R(t)
D(t)
u
u=0
products
reactants

(a)

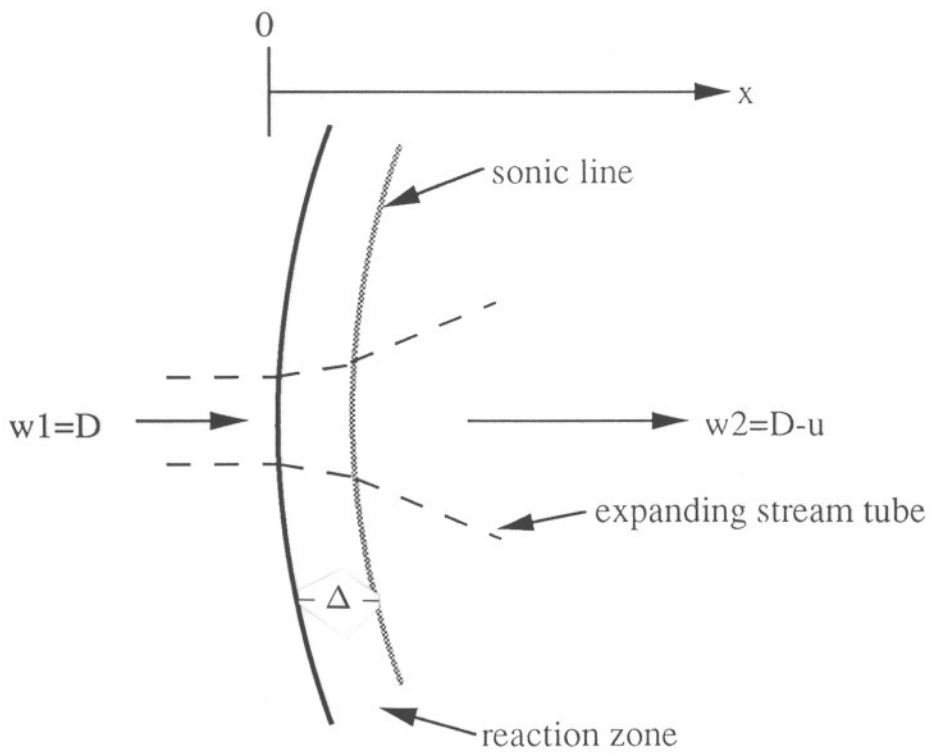
0
x
sonic line
w1=D
w2=D-u
expanding stream tube
Δ
reaction zone

(b)

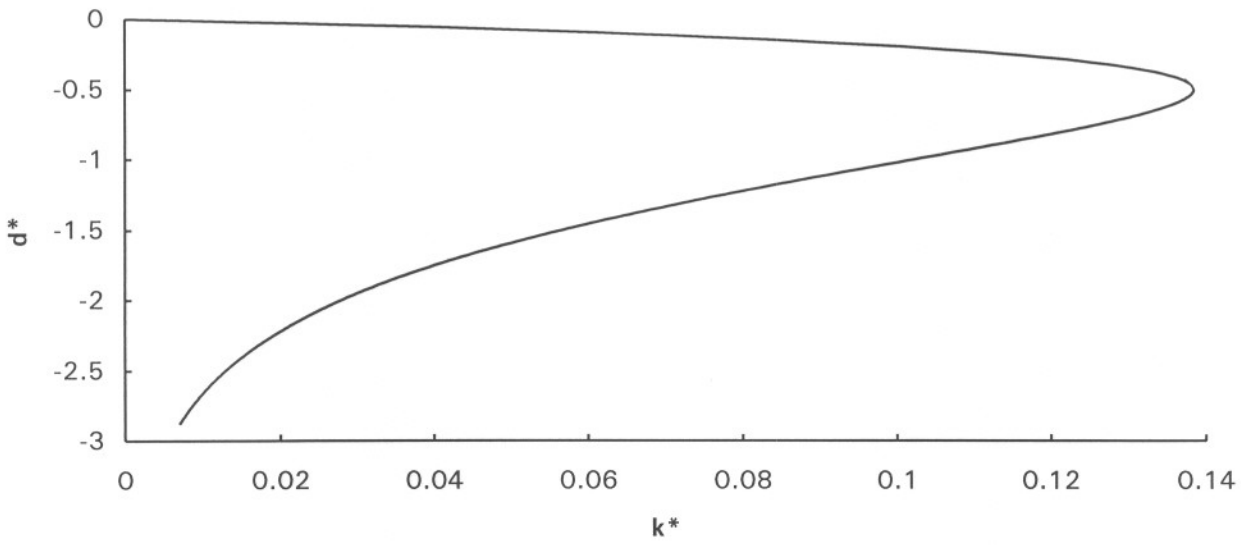
0
-0.5
-1
-1.5
-2
-2.5
-3
d*
0
0.02
0.04
0.06
0.08
0.1
0.12
0.14
k*

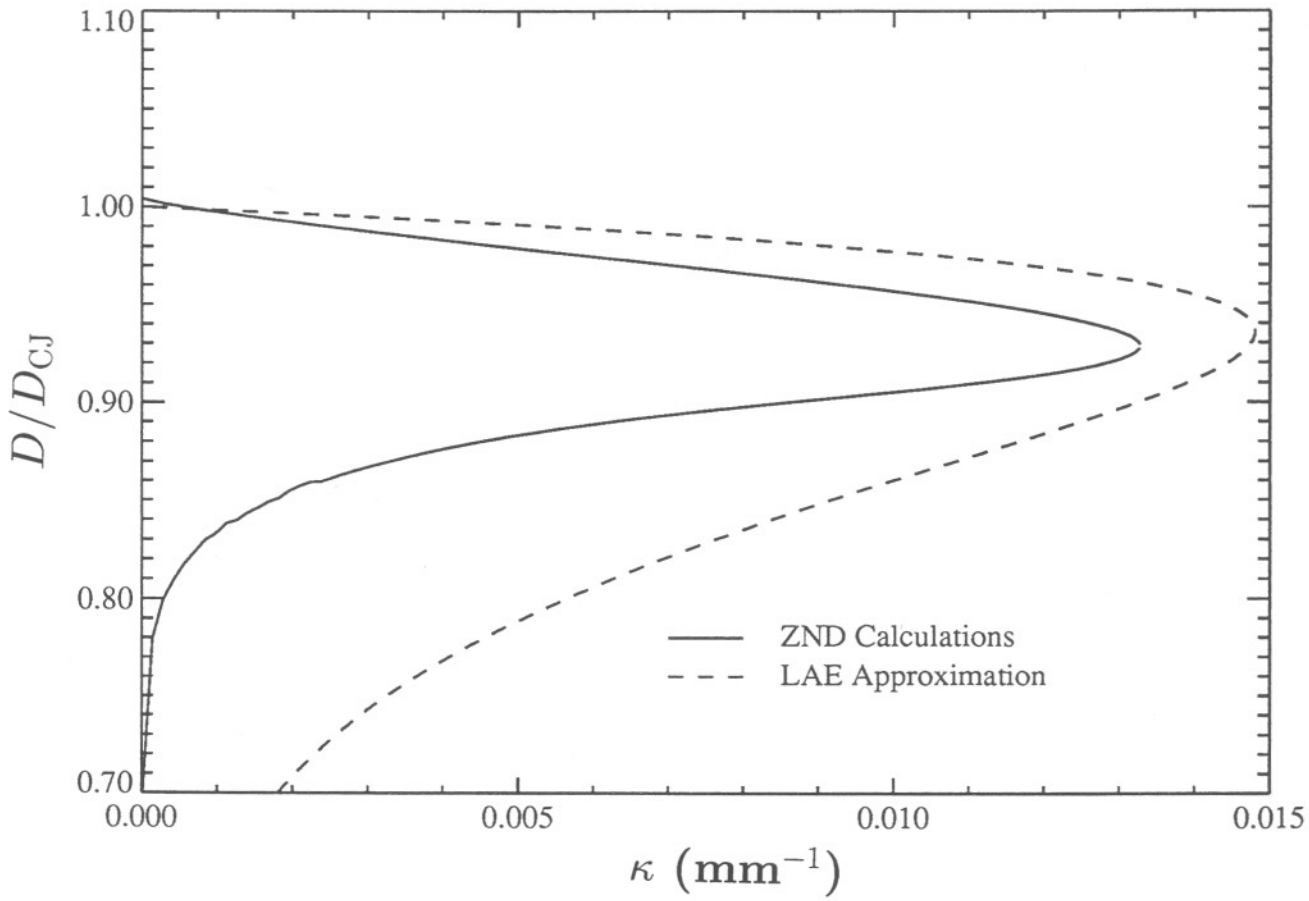
1.10
1.00
0.90
0.80
0.70
D/D_{CJ}
0.000
0.005
0.010
0.015
κ (mm^{-1})
ZND Calculations
LAE Approximation

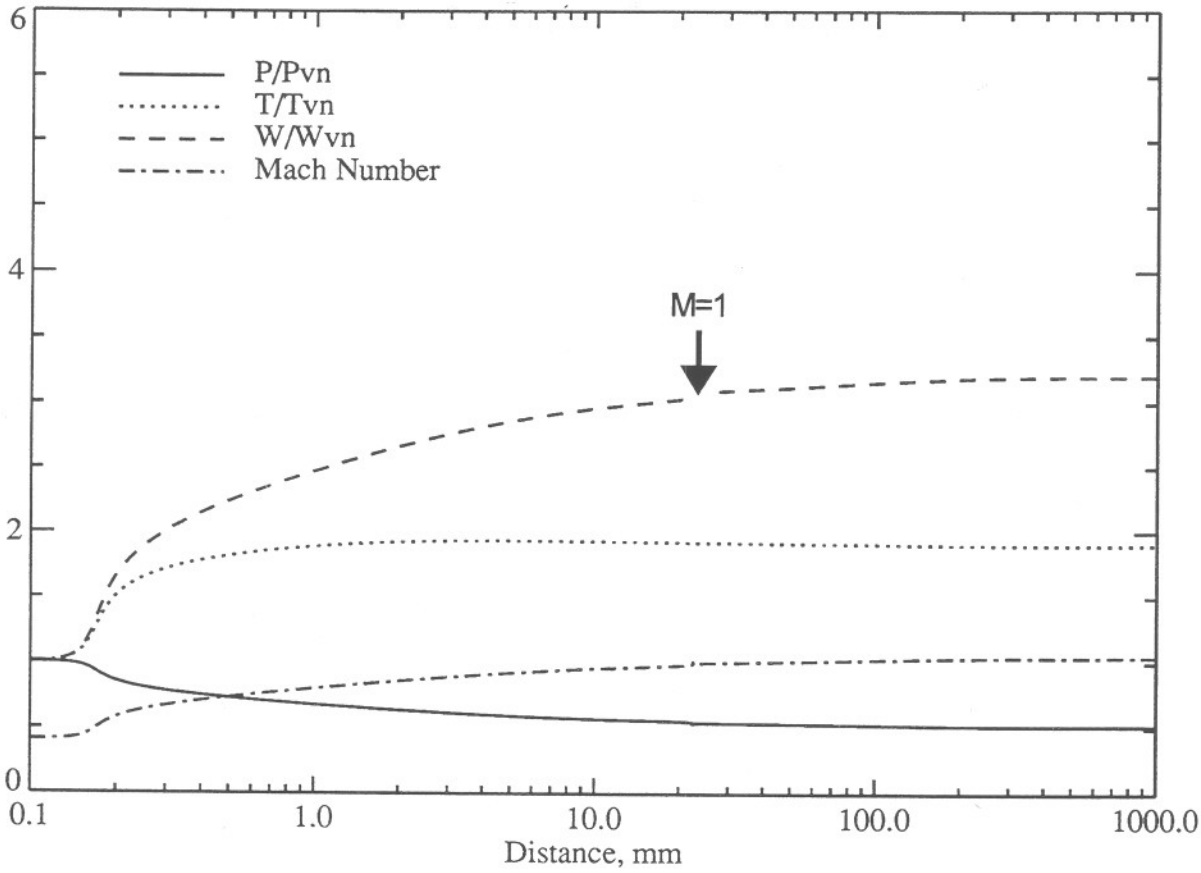
P/Pvn
T/Tvn
W/Wvn
Mach Number
M=1
6
4
2
0
0.1
1.0
10.0
100.0
1000.0
Distance, mm

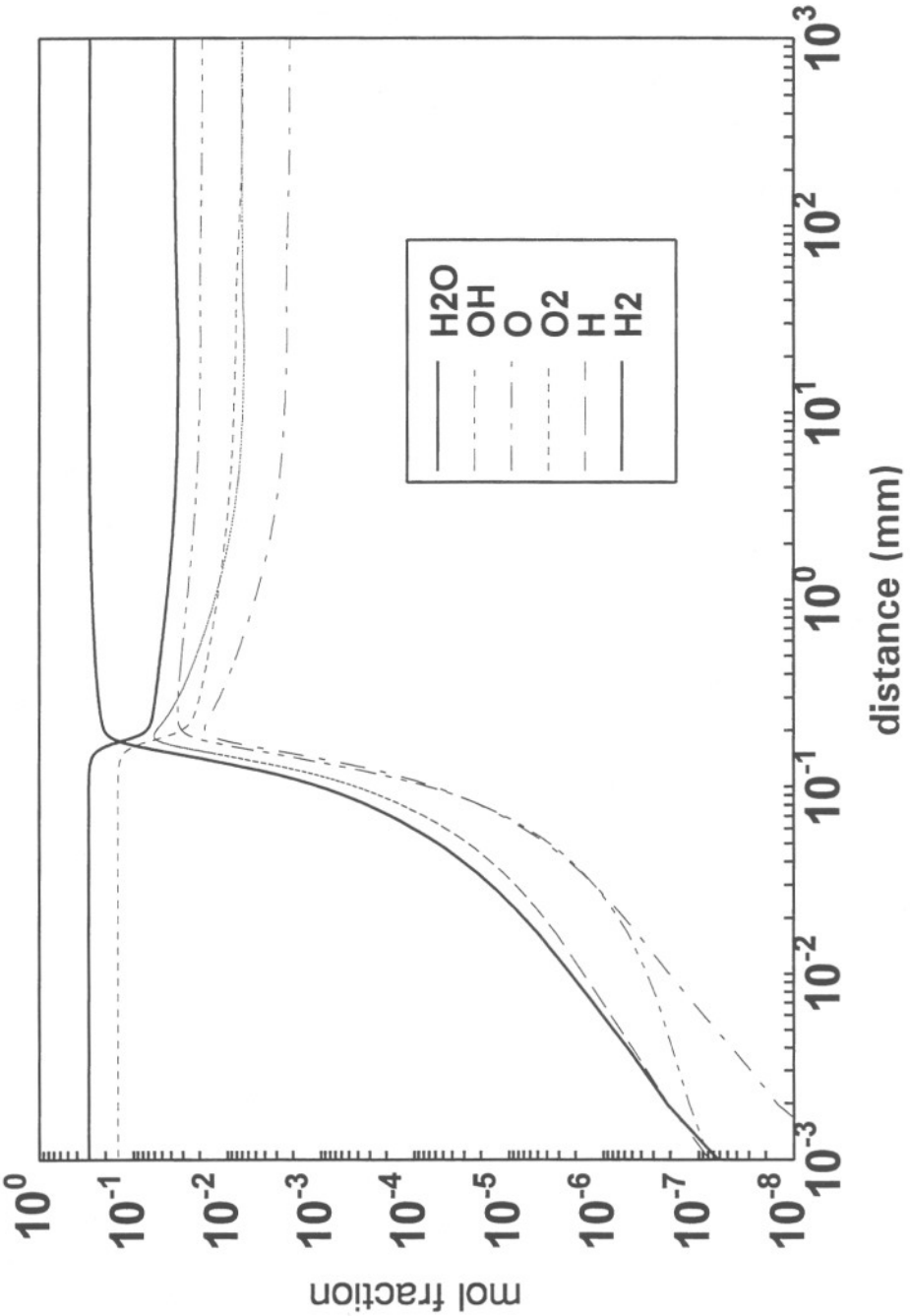
H2O
OH
O
O2
H
H2
mol fraction
distance (mm)
10^0
10^-1
10^-2
10^-3
10^-4
10^-5
10^-6
10^-7
10^-8
10^-3
10^-2
10^-1
10^0
10^1
10^2
10^3

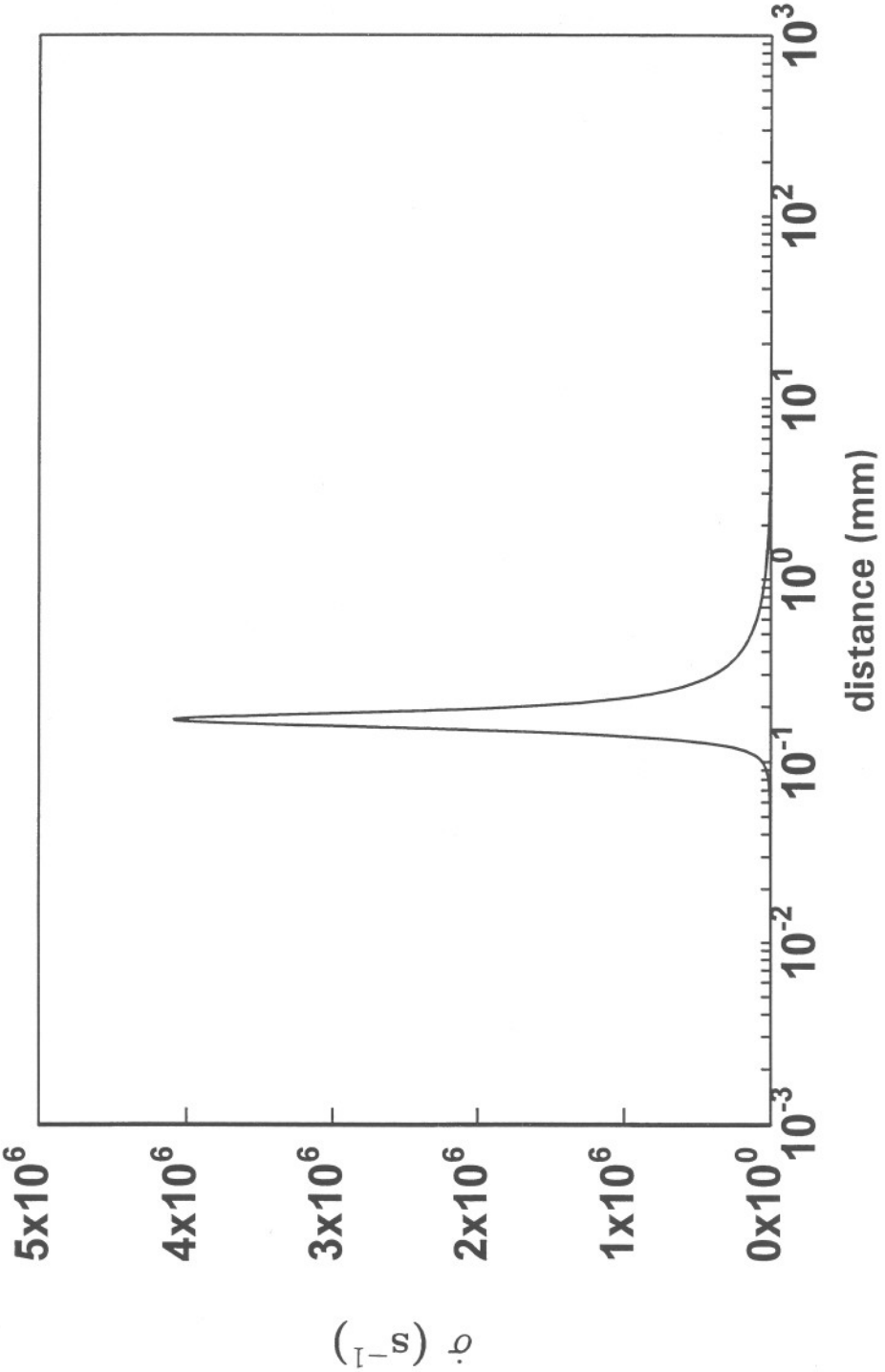
$\dot{\sigma}$ (s^{-1})
5x10^6
4x10^6
3x10^6
2x10^6
1x10^6
0x10^0
10^-3
10^-2
10^-1
10^0
10^1
10^2
10^3
distance (mm)

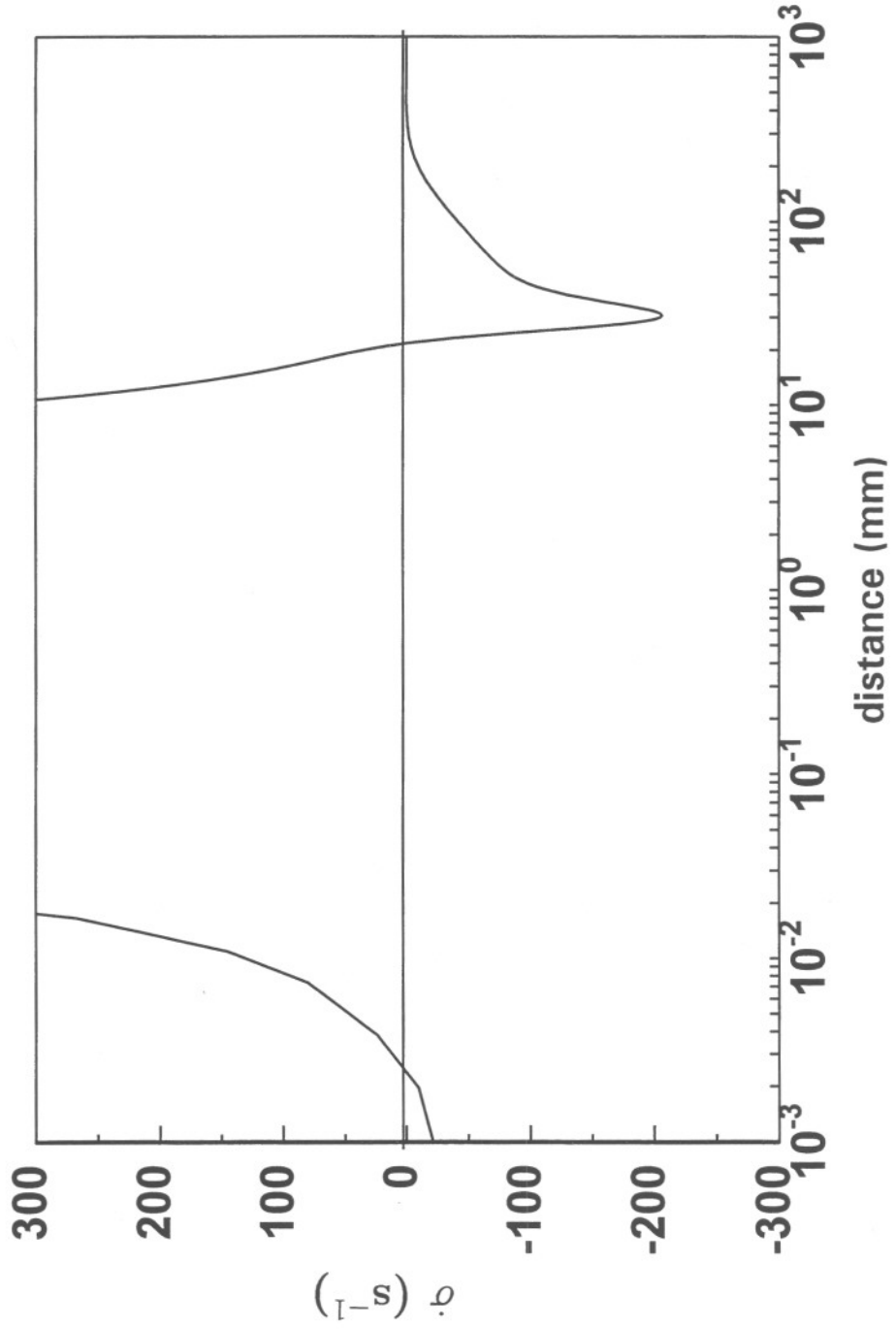
300
200
100
0
-100
-200
-300
$\dot{\sigma}$ (s^{-1})
10^{-3}
10^{-2}
10^{-1}
10^{0}
10^{1}
10^{2}
10^{3}
distance (mm)

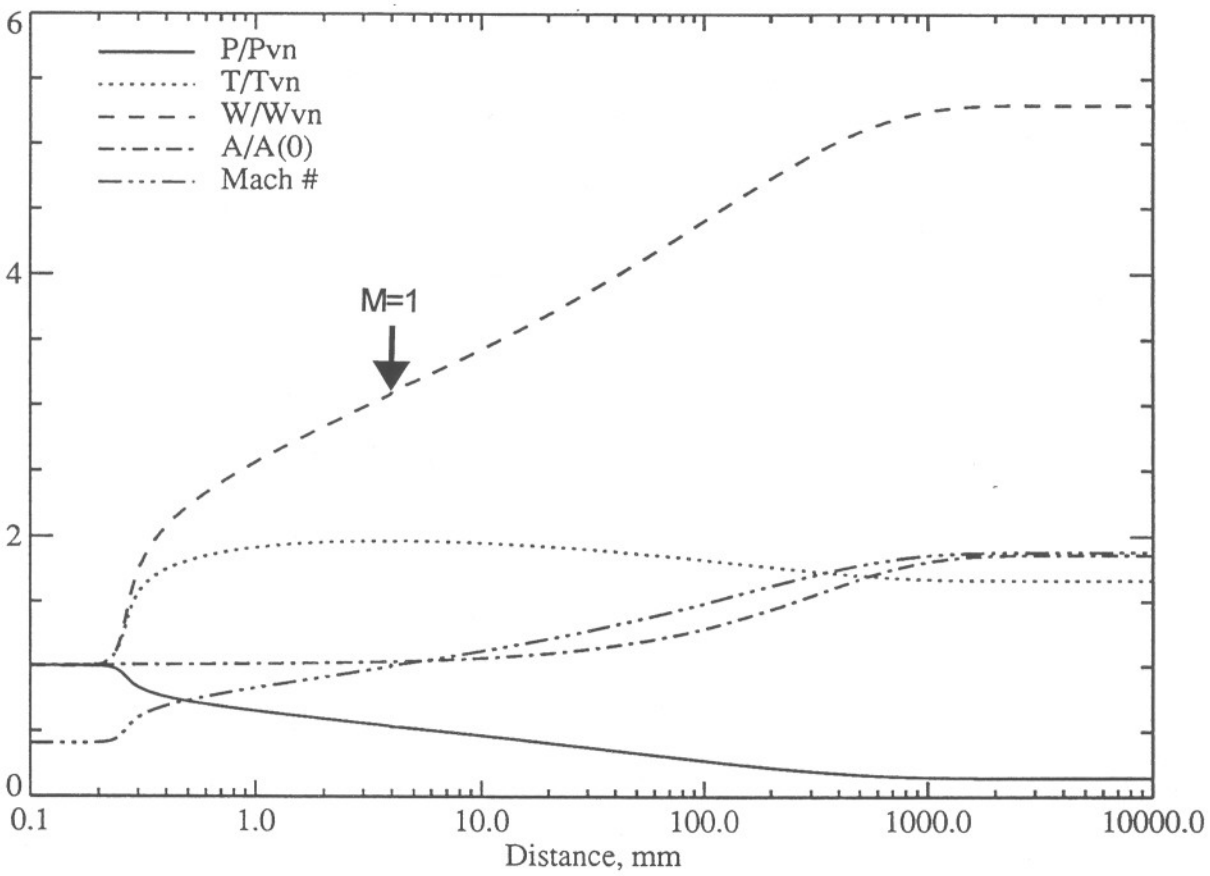
P/Pvn
T/Tvn
W/Wvn
A/A(0)
Mach #
M=1
6
4
2
0
0.1
1.0
10.0
100.0
1000.0
10000.0
Distance, mm

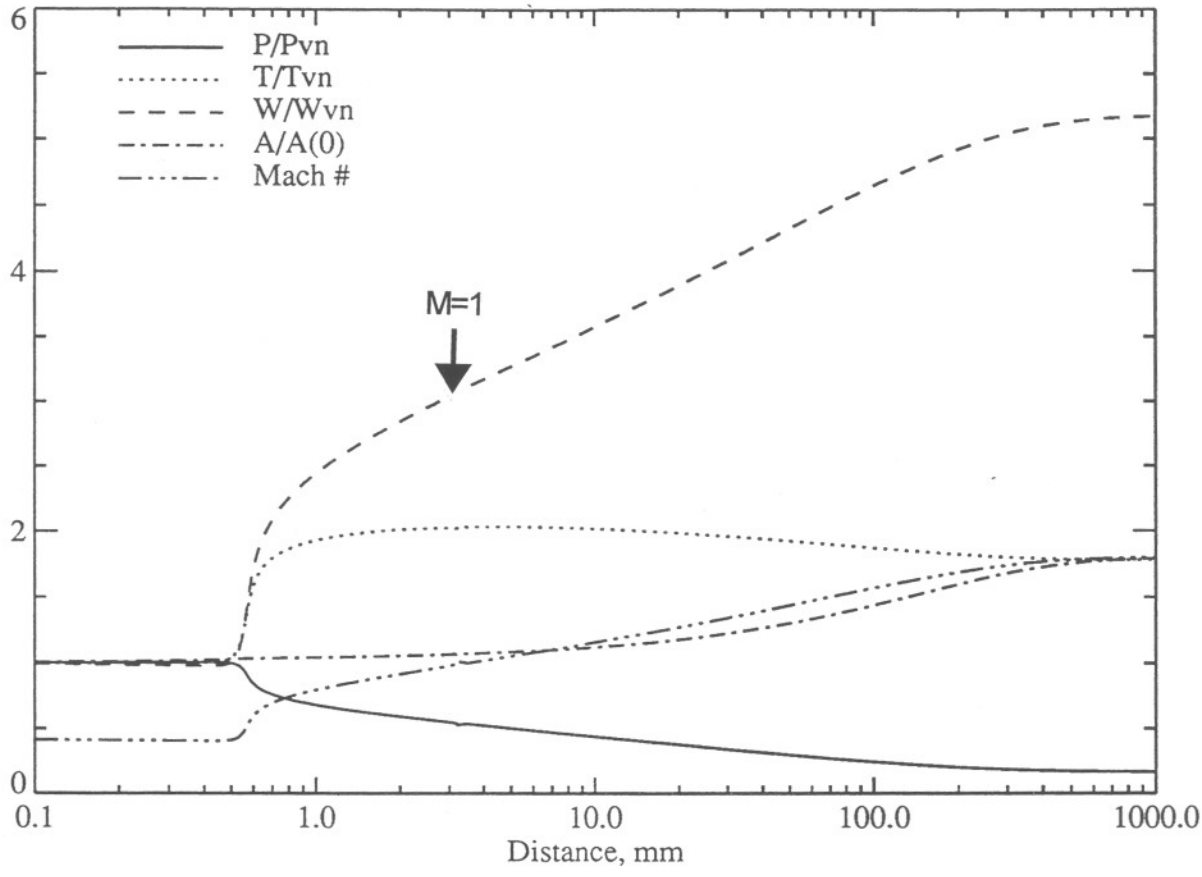
P/Pvn
T/Tvn
W/Wvn
A/A(0)
Mach #
M=1
6
4
2
0
0.1
1.0
10.0
100.0
1000.0
Distance, mm

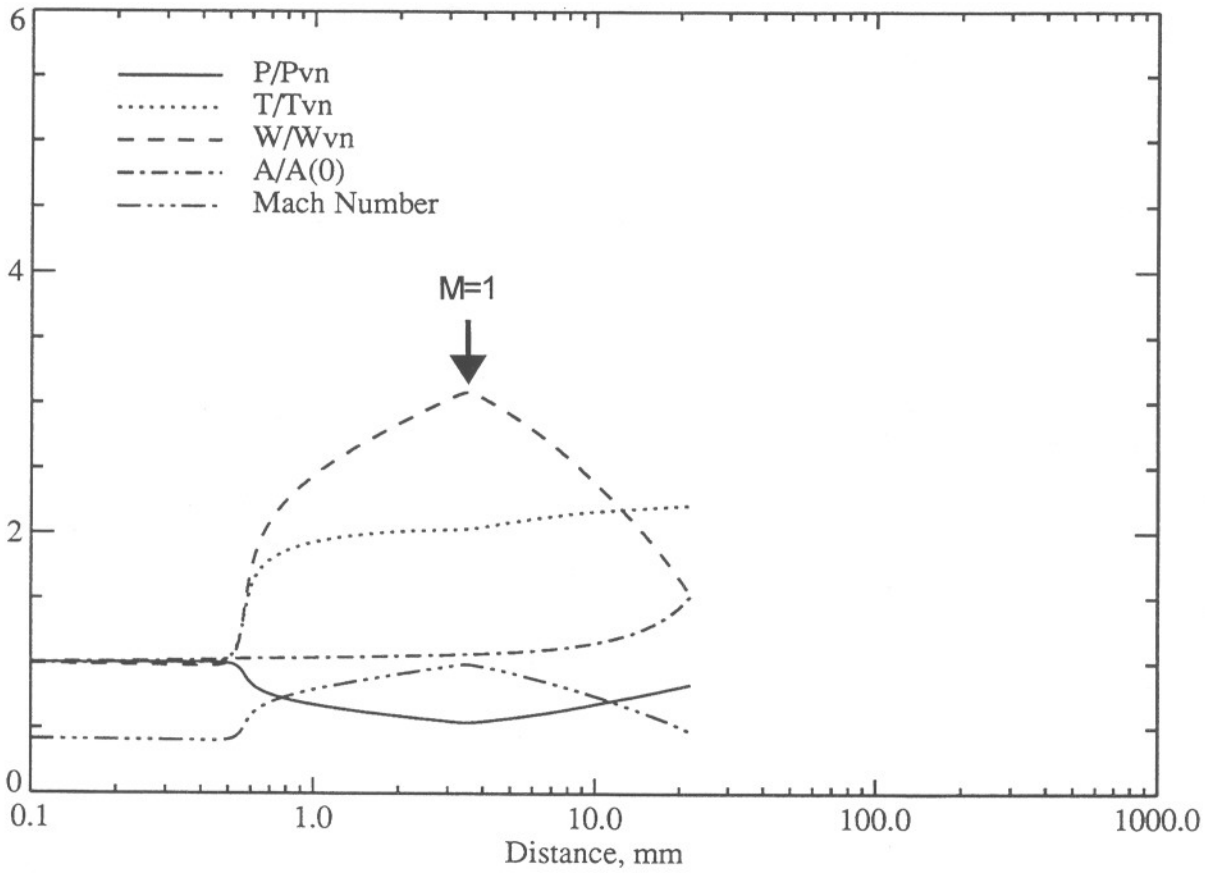
P/Pvn
T/Tvn
W/Wvn
A/A(0)
Mach Number
M=1
6
4
2
0
0.1
1.0
10.0
100.0
1000.0
Distance, mm

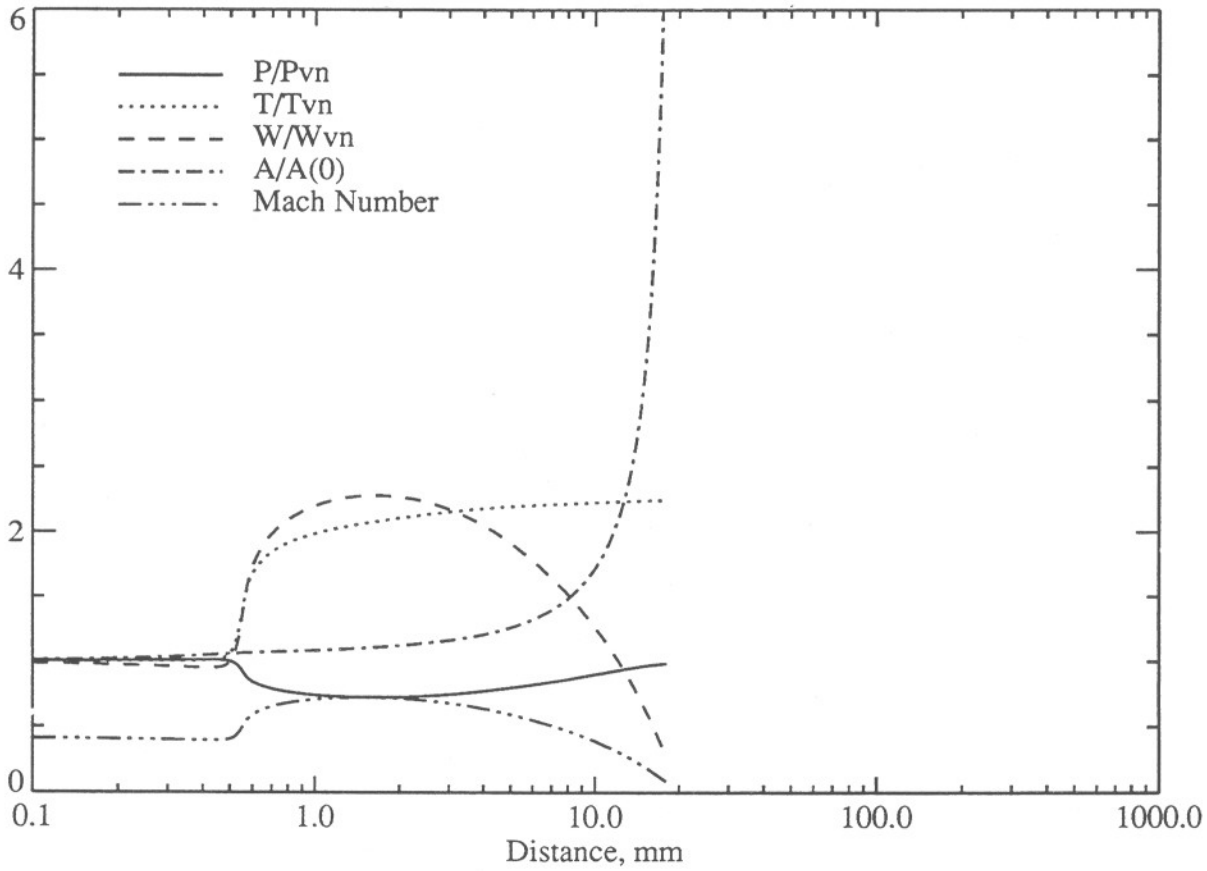
P/Pvn
T/Tvn
W/Wvn
A/A(0)
Mach Number
6
4
2
0
0.1
1.0
10.0
100.0
1000.0
Distance, mm

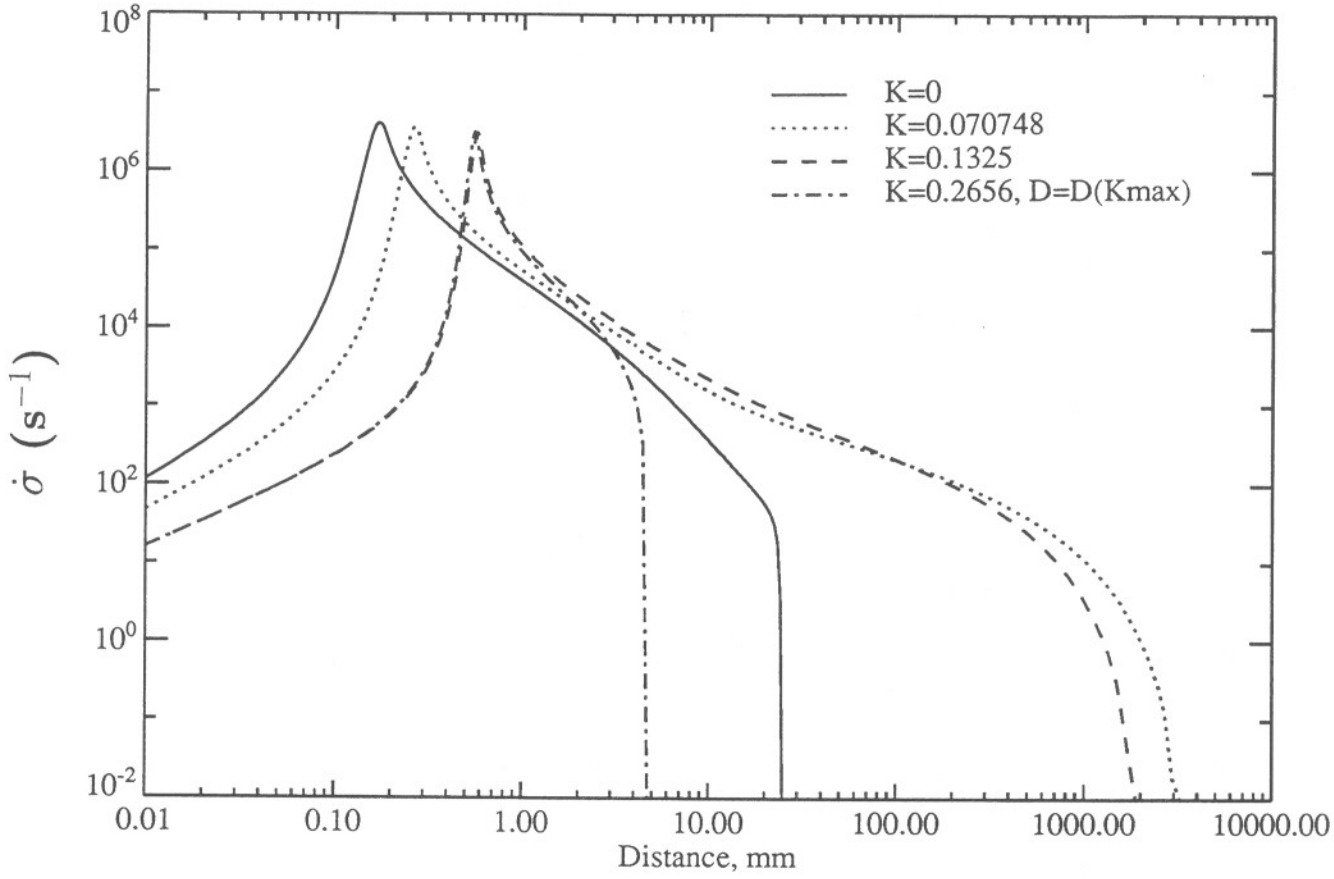
10^8
10^6
10^4
10^2
10^0
10^{-2}
$\dot{\sigma}$ (s^{-1})
K=0
K=0.070748
K=0.1325
K=0.2656, D=D(Kmax)
0.01
0.10
1.00
10.00
100.00
1000.00
10000.00
Distance, mm

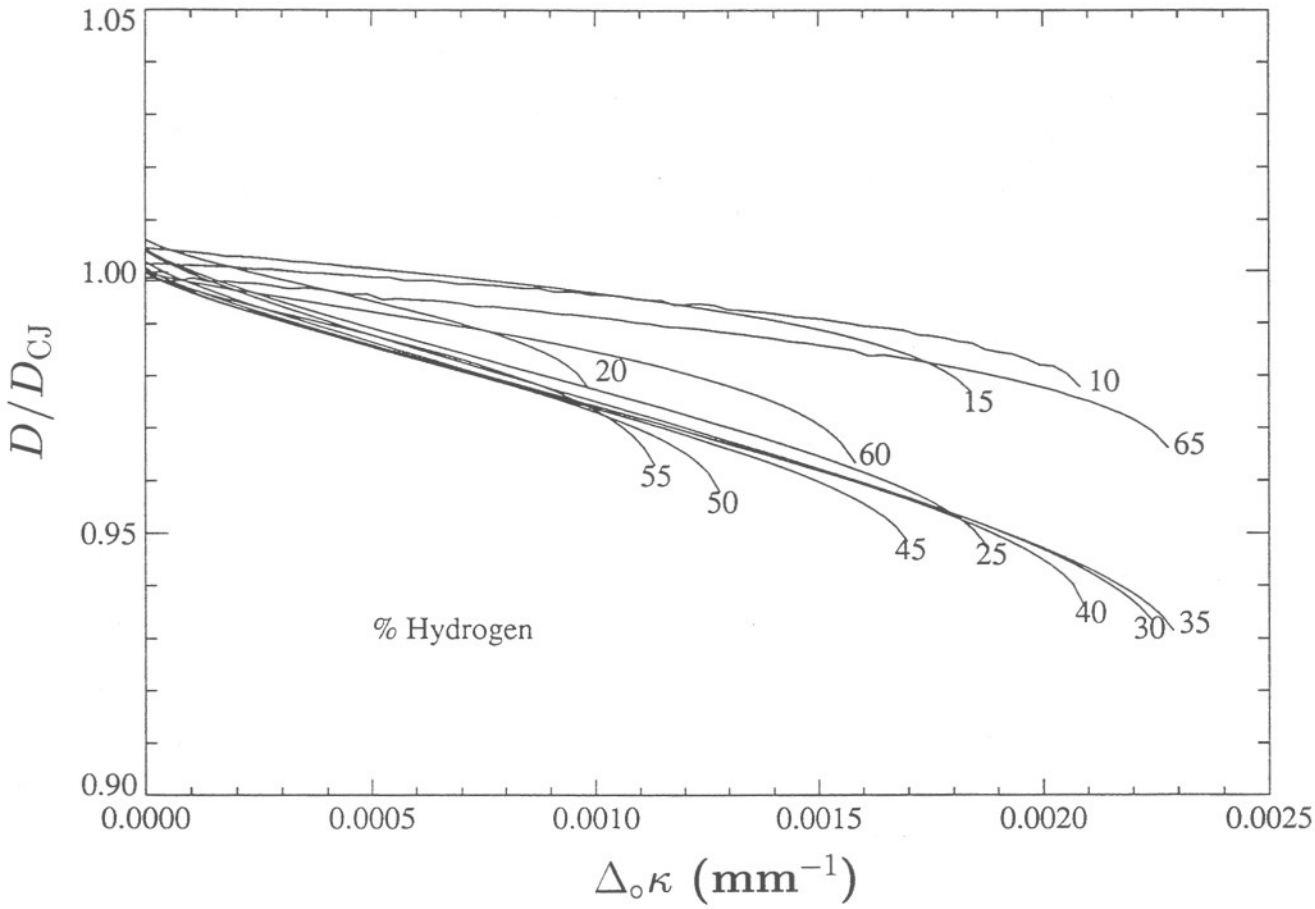
1.05
1.00
0.95
0.90
D/D_{CJ}
0.0000
0.0005
0.0010
0.0015
0.0020
0.0025
$\Delta_o\kappa$ (mm^{-1})
% Hydrogen
10
15
20
25
30
35
40
45
50
55
60
65

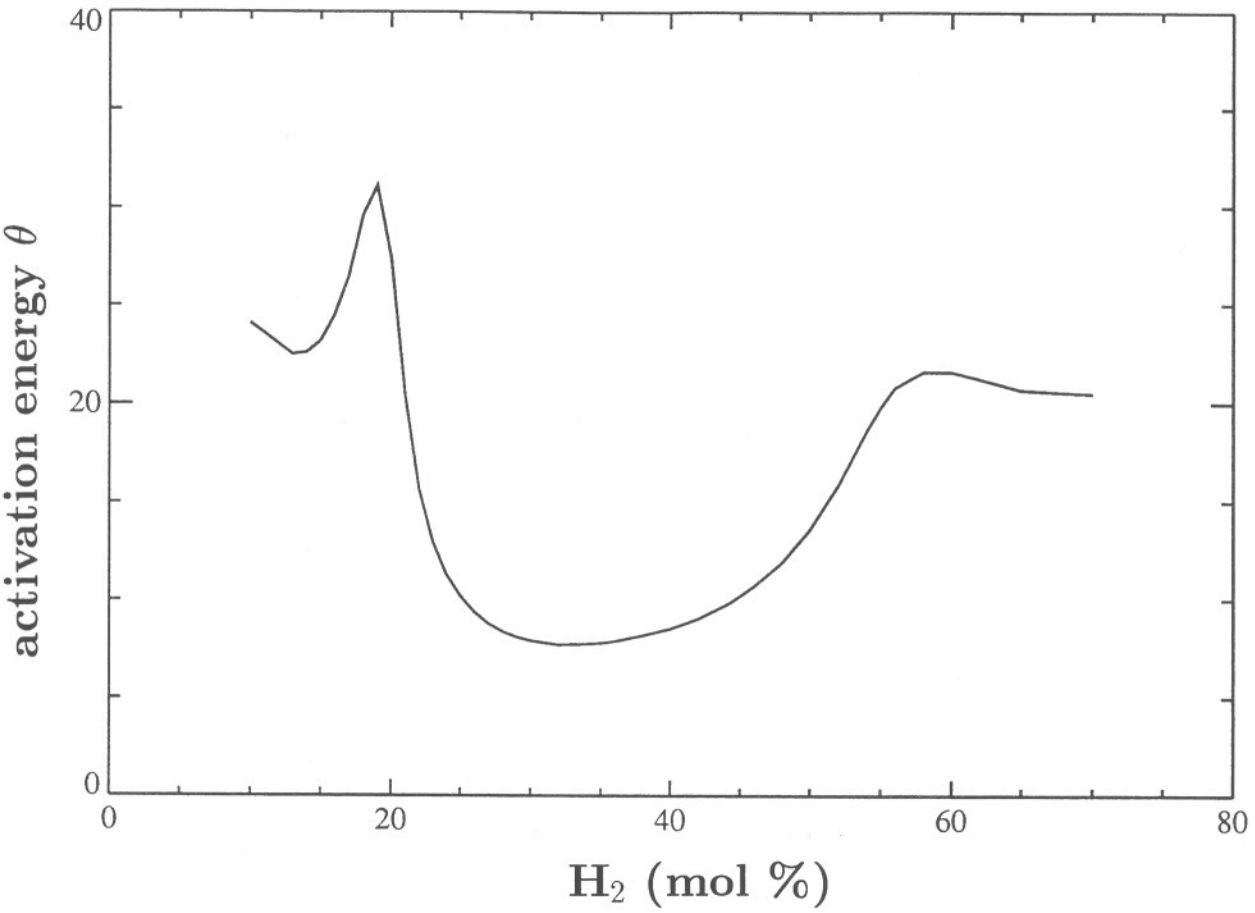
activation energy θ
40
20
0
0
20
40
60
80
H2 (mol %)

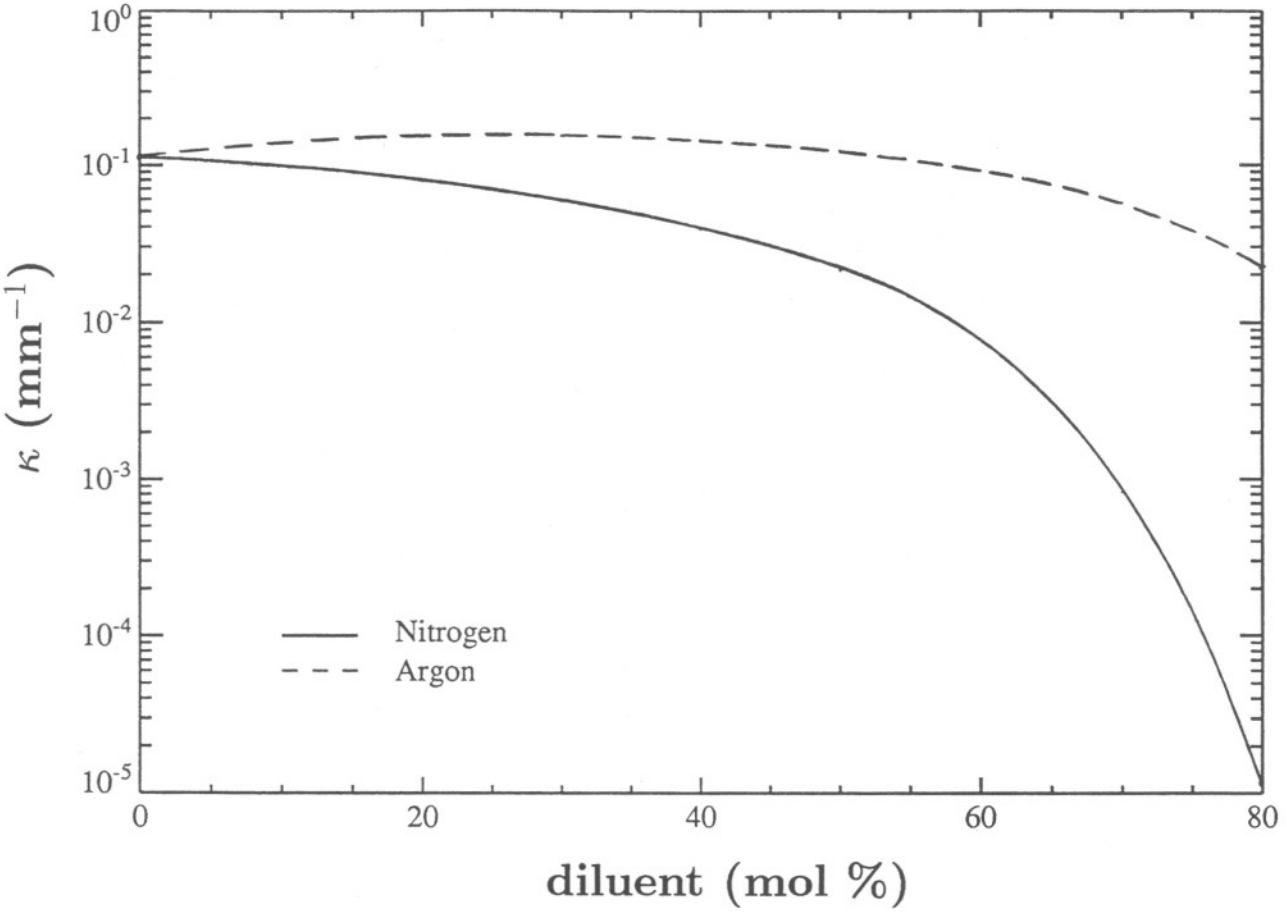
10^0
10^{-1}
10^{-2}
10^{-3}
10^{-4}
10^{-5}
κ (mm^{-1})
Nitrogen
Argon
0
20
40
60
80
diluent (mol %)

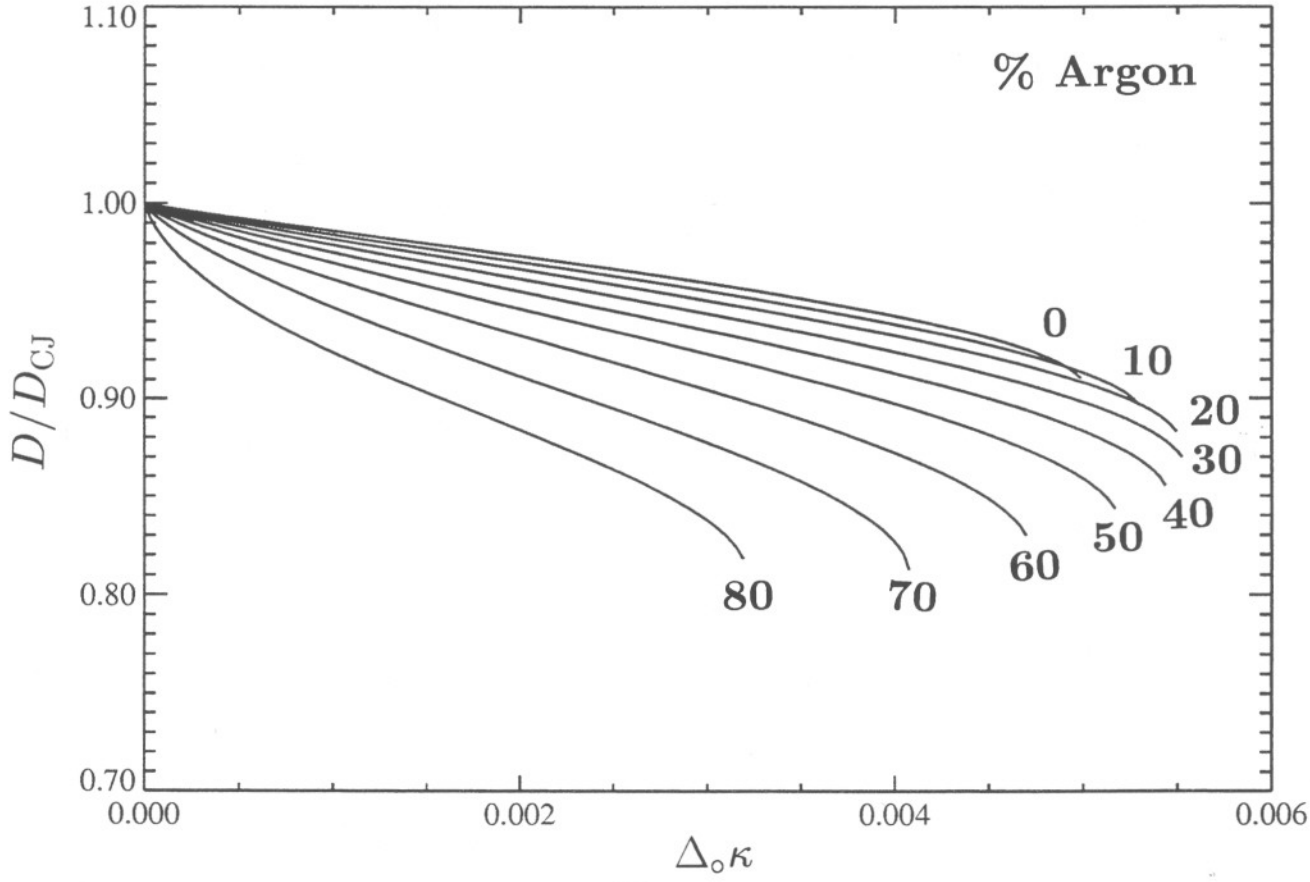
% Argon
0
10
20
30
40
50
60
70
80
1.10
1.00
0.90
0.80
0.70
0.000
0.002
0.004
0.006
D/D_{CJ}
$\Delta_o\kappa$

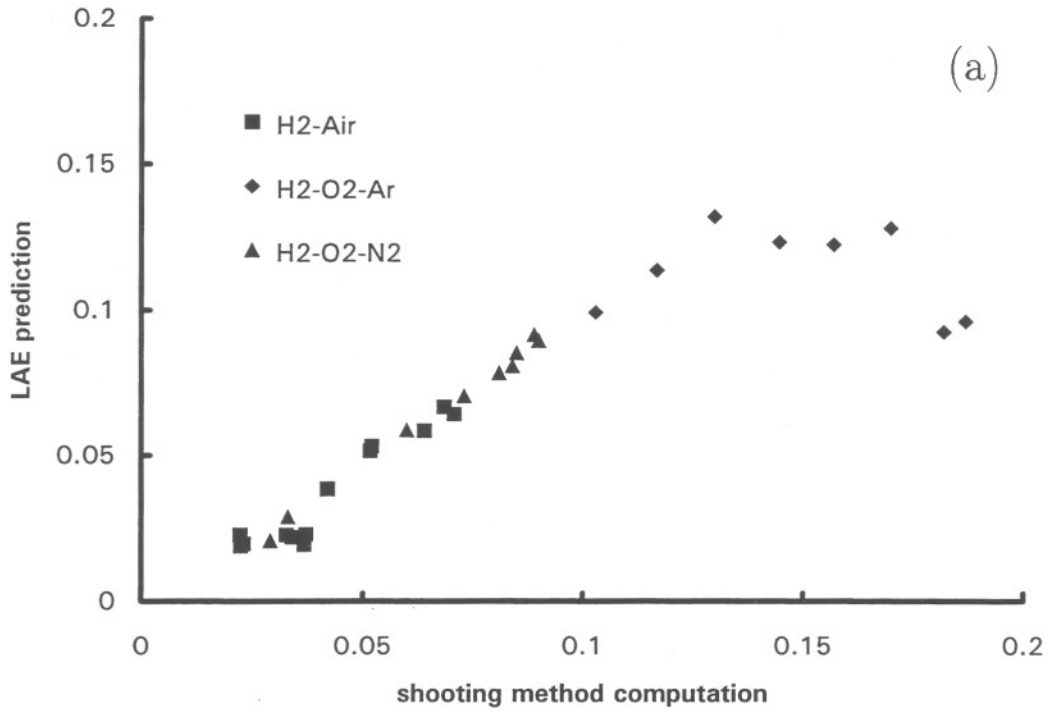
(a)
H2-Air
H2-O2-Ar
H2-O2-N2
LAE prediction
shooting method computation
0.2
0.15
0.1
0.05
0
0
0.05
0.1
0.15
0.2

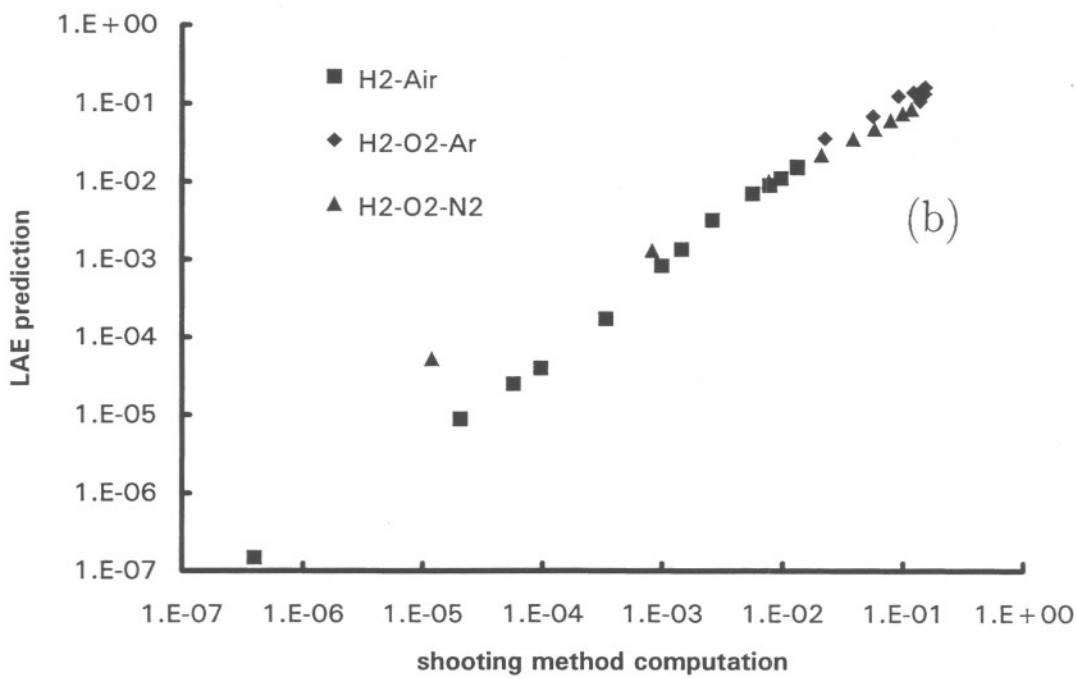
(b)
H2-Air
H2-O2-Ar
H2-O2-N2
LAE prediction
shooting method computation
1.E+00
1.E-01
1.E-02
1.E-03
1.E-04
1.E-05
1.E-06
1.E-07
1.E-07
1.E-06
1.E-05
1.E-04
1.E-03
1.E-02
1.E-01
1.E+00

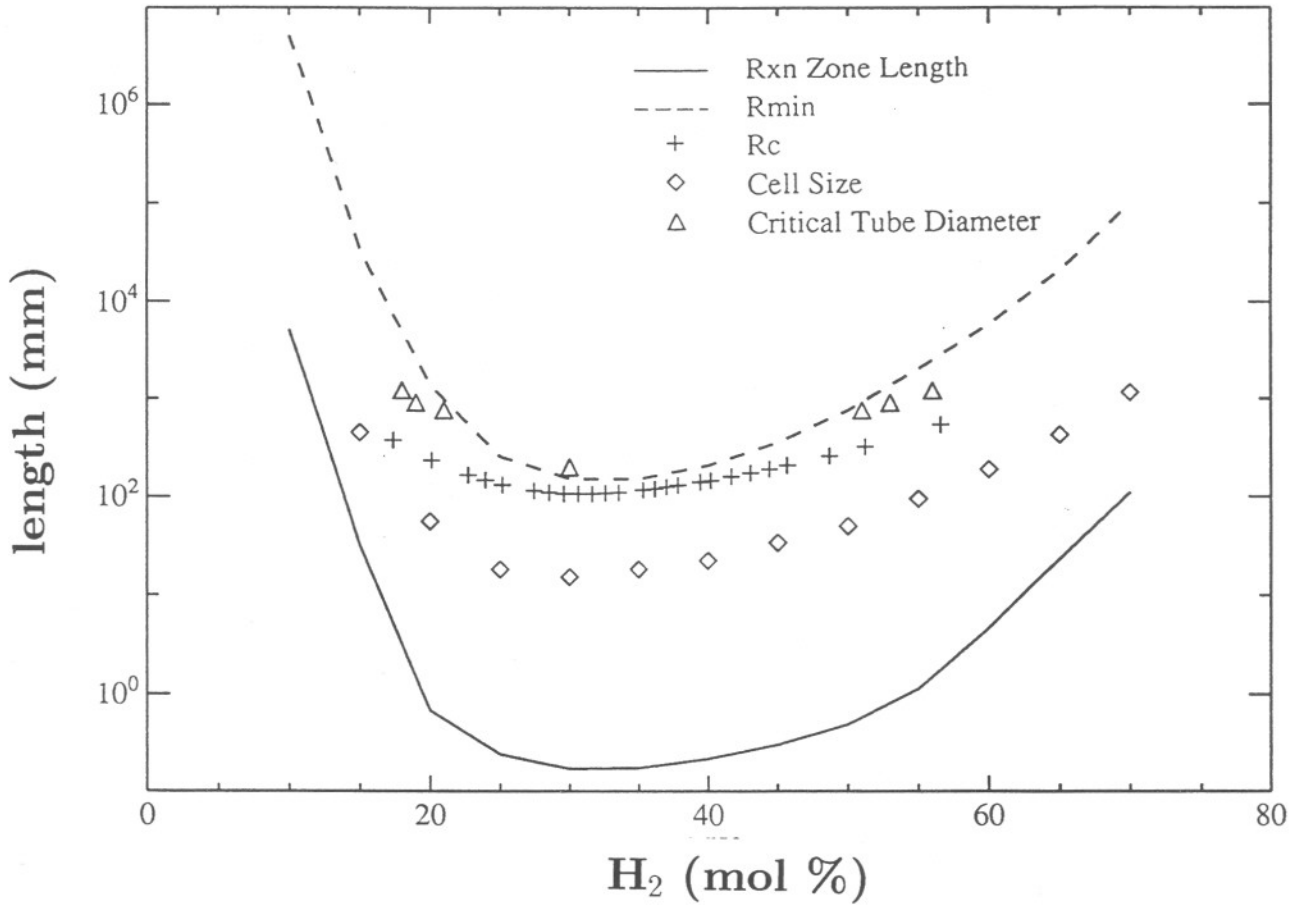
Rxn Zone Length
Rmin
Rc
Cell Size
Critical Tube Diameter
length (mm)
10^6
10^4
10^2
10^0
0
20
40
60
80
H_2 (mol %)

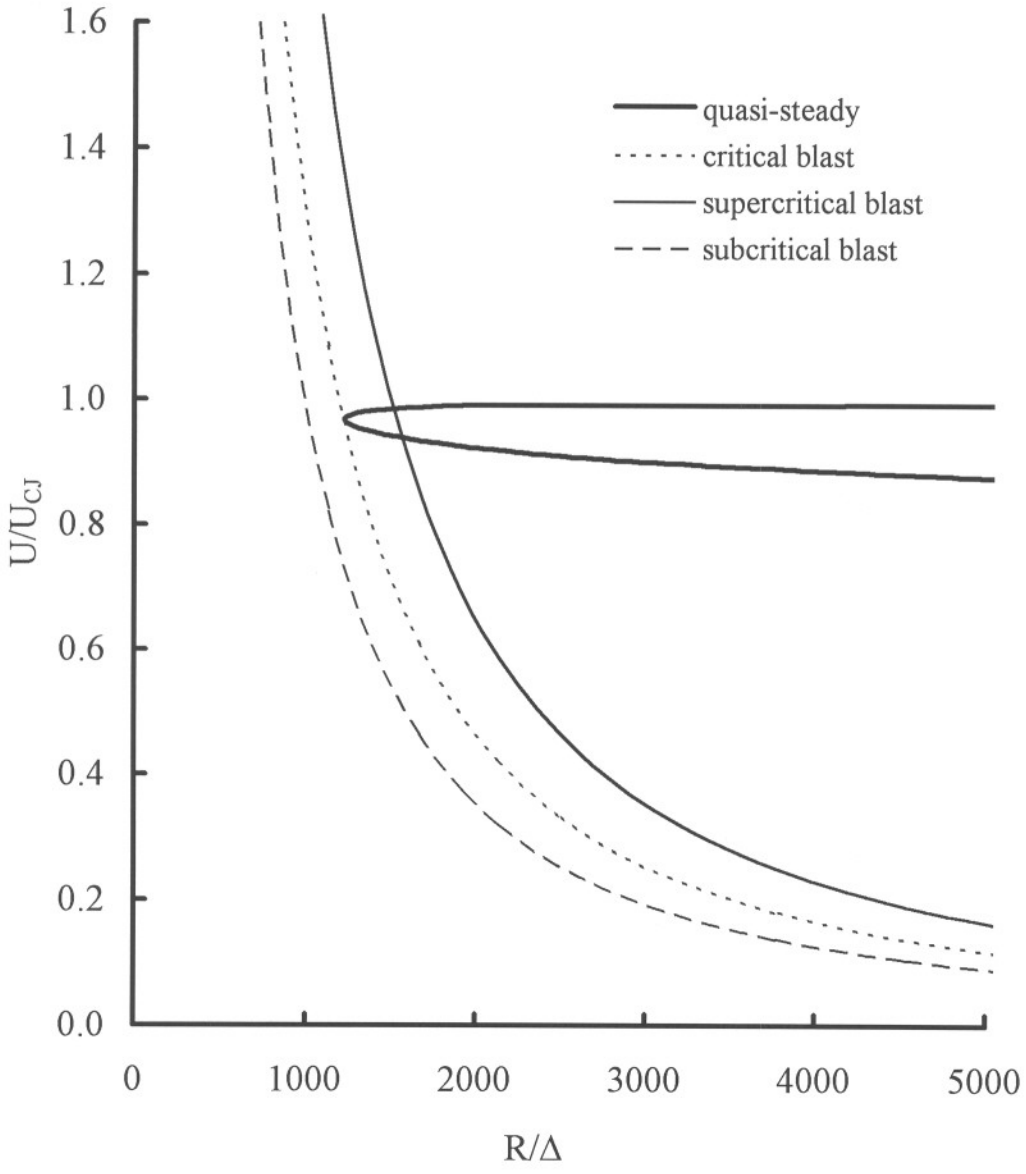
1.6
1.4
1.2
1.0
0.8
0.6
0.4
0.2
0.0
U/U_CJ
0
1000
2000
3000
4000
5000
R/Δ
quasi-steady
critical blast
supercritical blast
subcritical blast

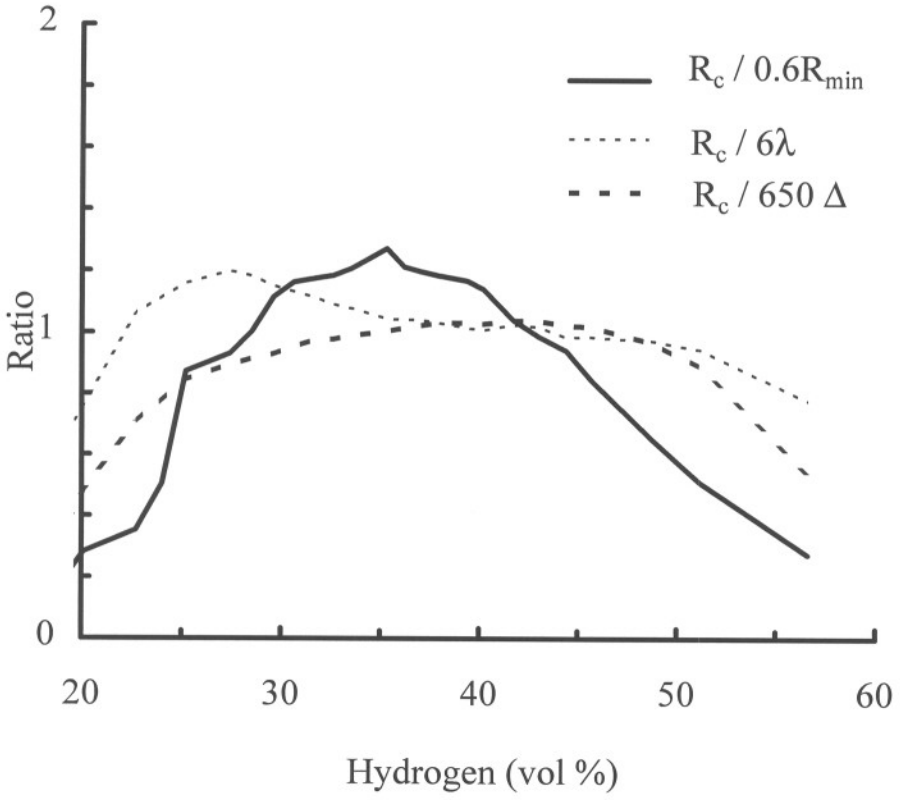
2
1
0
Ratio
20
30
40
50
60
Hydrogen (vol %)
R_c / 0.6R_{min}
R_c / 6λ
R_c / 650 Δ